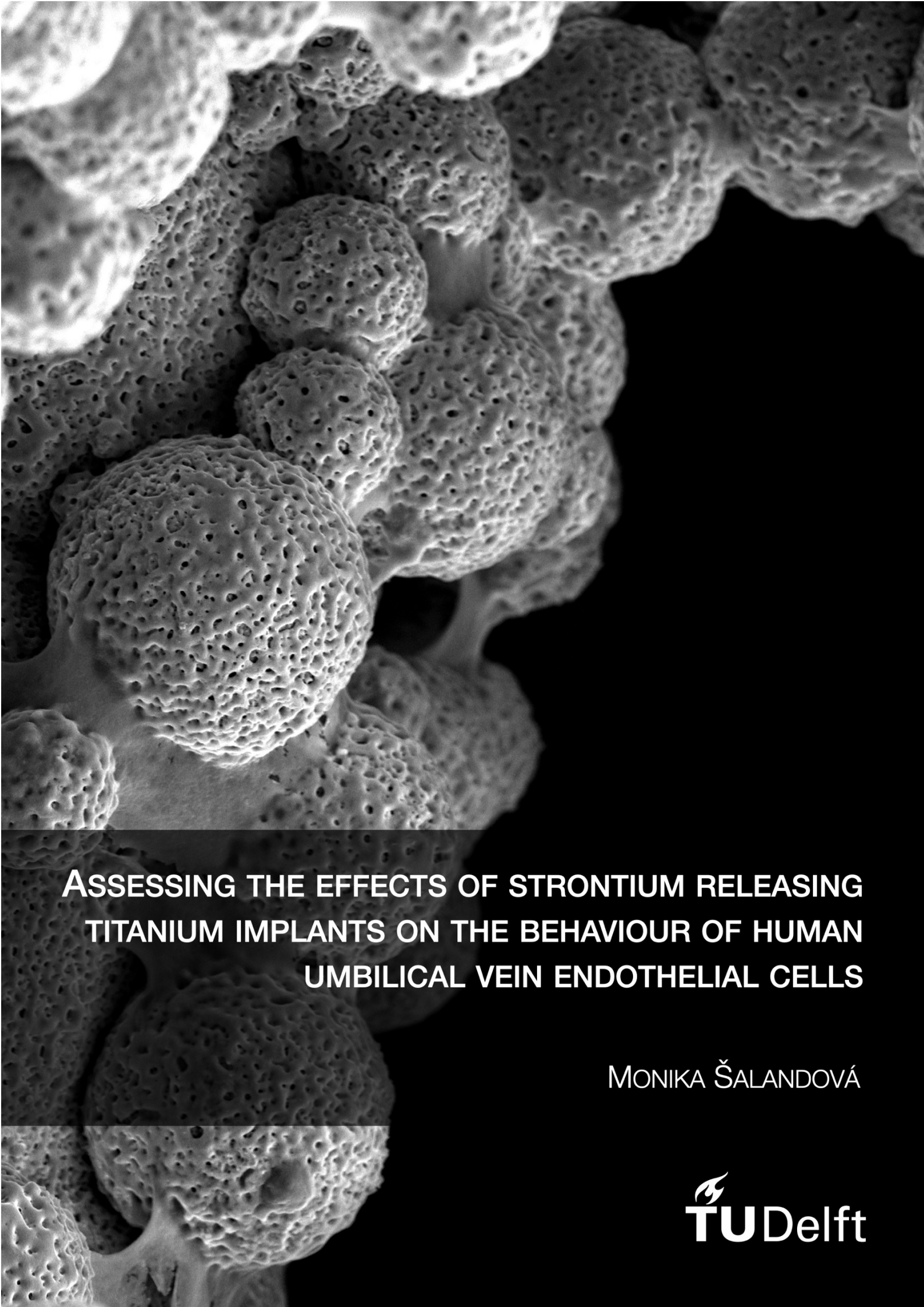

Assessing the effects of strontium releasing titanium implants on the behaviour of human umbilical vein endothelial cells

Monika Šalandová

TU Delft

ASSESSING THE EFFECTS OF STRONTIUM RELEASING TITANIUM IMPLANTS ON THE BEHAVIOUR OF HUMAN UMBILICAL VEIN ENDOTHELIAL CELLS

By

M. Šalandová

in partial fulfilment of the requirements for the degree of

Master of Science
in Biomedical Engineering

at the Delft University of Technology,
to be defended publicly on Wednesday December 16, 2020 at 11:00 AM.

Thesis supervisors:	Dr.ir. L.E. Fratila-Apachitei	TU Delft
	Dr. B.C.J. van der Eerden	Erasmus MC
	Ir. I.A.J van Hengel MSc	TU Delft
	Dr.ir. I. Apachitei	TU Delft
	Prof.dr. A.A. Zadpoor	TU Delft

This thesis is confidential and cannot be made public until December 16, 2023.

An electronic version of this thesis is available at http://repository.tudelft.nl/.

TU Delft

Acknowledgements

About three years ago, when I was contemplating my options for a master's degree in biomedical engineering, I settled my eye on TU Delft. At that time, I thought about how great it would be getting on board of one of those projects, which were within the scope of my interest of cell-material interaction, led by Dr.ir. Lidy Fratila-Apachitei. And here I am now, some (many many many) months later, defending my graduation project guided by her.

Therefore, I would like to express my sincere gratitude to my thesis supervisor, Dr.ir. Lidy Fratila-Apachitei, for the opportunity to work with her, contribute to this project and learn more about the principles of cell-material interaction. She was a great enthusiastic guide providing me with immense support and never-ending encouraging words every step on the way, especially in the most needed moments.

Due to the collective work of TU Delft and Erasmus MC on this project, I had a chance to work also in the Laboratory of Calcium and Bone Metabolism and check off one of my practical goals for the two years at TU Delft; to acquire laboratory skills in cell culturing which I could then utilize in testing of new biomaterials. Hereby, I would like to thank Dr. Bram van der Eerden for giving me the privilege to be trained by the best, learn not only the good laboratory practices but also expand my knowledge about cellular biology of bone healing. His door was always open (literally) for any questions and he was always ready to discuss and share his expertise.

My special thanks go also to my daily supervisor, Ir. Ingmar van Hengel MSc, who took care of all the necessary lab trainings at TU Delft facilities and helped me with planning of the experiments. I would like to also express my appreciation to Dr.ir. Iulian Apachitei for sharing his know-how and taking time to participate in all the meetings we had throughout the year.

I cannot thank enough Marijke Koedam, who trained me in the cell culture lab from point zero to being sufficiently independent during my internship, and Michelle Minneboo who provided subsequent practical support during the graduation project. My special thanks go also to Shuang Zhang, for all the protocols and practical knowledge about the work with HUVECs that she has shared. Last but not least, I would like to also thank Sander Leeflang, Michel van den Brink, and Ruud Hendrikx for their technical support at the TU Delft facilities during the project.

I would not be able to get this far without having my parents and my sisters by my side. I cannot thank enough my mom and dad for the 20 years of continuous support of my "educational career", for giving me the chance to go and learn while exploring the world. Although I am not sure whether they finally remember what I do now, they all have always had my back and were ready to hear about all the ups and downs of my (student) life. I am also extremely grateful for my "other" family, Joelene, Todd, and Cece, who have been part of my journey despite the great distance and always excited to hear news about my progress and future plans.

Finally, I would like to thank my amazing friends, Priyanka and Magdalena, for their support every step on the way, all the walks and tea breaks, and for being the best companions one might ask for (not only for the academic life), Bogdan for his (entertaining) company in the CCB lab, and all others who shared with me the countless moments of frustration and joy and became an inherent part of this unforgettable TU Delft adventure.

Abstract

Introduction: Aseptic loosening of an orthopaedic implant due to the unsatisfactory attachment to the bone remains one of the most common reasons for failure of these implants. One of the possible approaches for improving the connection between the implanted biomaterial and the bone tissue being formed is the incorporation of bioactive agents onto the surface of the biomaterial to promote bone and blood vessel formation. This work investigated the effects of strontium (Sr), a known osteogenic and angiogenic agent, incorporated in surfaces of 3D printed titanium implants on the behaviour of human umbilical vein endothelial cells (HUVECs), to determine its potential role in improving osseointegration by promoting an early development of a well vascularized bone.

Methods: 3D printed titanium implants were subjected to plasma electrolytic oxidation (PEO) in electrolytes with and without Sr addition. The effects of Sr incorporated on the surfaces were subsequently tested *in vitro* by assessing the morphology, proliferation, wound healing ability and angiogenic potential of HUVECs. In addition, a coculture model with conditioned medium from mesenchymal stromal cells (MSCs) was included for investigations of the angiogenic potential.

Results: The characterization of the PEO-treated titanium implants confirmed comparable topography and distinct chemical composition of samples treated in electrolytes without (PT) and with Sr (PT-Sr). Despite the good initial attachment, HUVECs showed a tendency to gradually leave both PT and PT-Sr implants. No improvement in proliferation of HUVECs seeded on PT-Sr implants was observed, yielding comparable results with the PT implants. The ions released from the PT and PT-Sr surfaces did not instigate faster wound healing ability of HUVECs and the direct contact of cells with the surfaces did not elicit paracrine signalling which would contribute to faster closure of the wound. The coculture model revealed higher angiogenic potential of HUVECs seeded on the PT and PT-Sr surfaces when cultured in the presence of conditioned media obtained from MSCs, implying the importance of interactions among these cell types for achieving successful bone repair.

Discussion and conclusions: Comparison of the obtained data and evidence found in the literature implied that the 3D printed and PEO-treated implants could not support thriving of endothelial cells, most probably due to the topography and associated roughness of the surfaces given by the method employed for the 3D printing of these implants. However, with consideration to the physical and chemical complexity of the implants, further tests will have to be conducted to validate these assumptions.

Table of contents

1 Introduction

Despite the great technological advancements in biomaterials, implant design and orthopaedic surgery over the past decades, implant failure remains a concern for approximately 10% of patients undergoing primary total hip arthroplasty (THA) [1,2]. Many of the causes leading to failures are attributed to poor or delayed osseointegration of the implants [2,3], as it has been established that achieving osseointegration is a key prerequisite for implant stability and proper loading of the implant [2,4,5]. Unsatisfactory osseointegration is often associated with the formation of fibrous tissue between the biomaterial and the bone, which represents a soft interlayer not able to sufficiently anchor the implant. Moreover, an unsecured attachment can result in micromovements and subsequent generation of wear debris, which may elicit an inflammatory reaction and excessive bone resorption, eventually leading to the loosening of the implant [6–10].

Titanium alloys are increasingly used biomaterials for total joint replacements (TJRs). They are often praised for their high corrosion resistance and moderate elastic modulus, the latter reducing the stress shielding effect and preventing undesired bone resorption [6,7,9]. Even though these biomaterials exhibit an exemplary chemical and mechanical stability, their bioinert nature does not encourage the establishment of a stronger and more physiological connection between the implant and the new bone, thus necessitating further surface treatment of the implants [2,10,11]. Many of the approaches currently used to promote osseointegration are based on the attraction of mesenchymal stromal cells (MSCs) and the stimulation of their osteogenic differentiation, leading to new bone tissue formation on the implant surface. This can be achieved through the adjustment of the chemical and physical surface properties of the used biomaterial [2,4,6].

Given the highly vascularized nature of the bone [12,13] and the importance of blood supply in the bone repair process [14], angiogenesis represents an apparent target and remains a major challenge in bone tissue engineering and regeneration therapies. Due to their vital role, damaged blood vessels are repaired in the initial stages of bone regeneration [5,15,16], restoring the blood flow and thereby ensuring delivery of oxygen, nutrients, and signalling molecules as well as facilitating the supply of cells to the affected site and enabling the removal of waste products [17–19]. Implants with both osteogenic and angiogenic surface biofunctionalities are, therefore, highly desirable to enhance osseointegration [20].

The research on the effects of biomaterial's physical and chemical properties on angiogenesis is relatively scarce when compared to the research on osteogenic agents [21]. Among the available methods used for the modulation of cellular responses by an implant, modification of the chemical composition of the biomaterials is an approach that enables the incorporation of multiple agents with different action mechanisms, thereby yielding a biomaterial with versatile surface properties. Essential and trace elements are known for their inherent role in many molecular mechanisms in the human body, and the increased understanding of their signalling and structural functions associated with bone metabolism has led to their utilization in therapeutic applications for bone (*e.g.*, osteoporotic treatments, promoting osseointegration) [5,12,13,22]. Nowadays, elements such as strontium (Sr), which may additionally enhance angiogenesis [23], are also incorporated into bulk biomaterials or onto their surfaces, delivering their stimulatory effect to the intended site through tuneable release kinetics. Results of a conducted literature review revealed that the presence of a carefully chosen concentration of strontium possesses beneficiary effects for the proliferative and migratory activity of

human umbilical vein endothelial cells (HUVECs) and guides their angiogenic differentiation [21,23–30]. Therefore, such biomaterials could modulate the activity of stem/progenitor cells, thereby inducing new bone and/or blood vessel formation and enhancing osseointegration [5,12,22,31,32].

The aim of this project was to assess the effects of Sr incorporated on the surface of 3D printed titanium implants on the behaviour of HUVECs. For incorporation of Sr on the implants, plasma electrolytic oxidation (PEO), which generates a porous oxide layer through local plasma discharges, was selected [33,34]. This method requires a short procedure time, allows incorporation of a wide range of elements/molecules (including strontium) in the growing porous oxide layer and can be applied for geometrically complex titanium substrates [35–39]. Previous research performed in our group using this surface treatment in Ca and P bearing electrolytes demonstrated the ability of the resultant surfaces to support differentiation and matrix mineralization of stem/osteoprogenitor cells. In addition, incorporation of Ag nanoparticles provided antibacterial properties to the surfaces thus being able to fight the implant associated infections [39]. Additional angiogenic activity of such surfaces would further enhance the clinical performance of such implants.

The effects of the developed bioactive system on HUVECs were tested *in vitro.* The cellular morphology, proliferative and migration behaviour and angiogenic differentiation were tested using relevant assays. To acknowledge the complexity of the signalling pathways involved in the fracture healing process and approximate the biomolecular interactions occurring during the mutually dependent processes of vessel and bone formation, coculture experiments with MSCs were also performed.

2 Materials and Methods

2.1 Preparation and characterization of strontium releasing surfaces

2.1.1 Implant fabrication

Highly porous implants were produced through scanning laser melting (SLM) 3D printing method. The fabrication followed a previously described design published by van Hengel *et al.* [40], developed with consideration to the limitation of the 3D printing process, and desired surface area and porosity. Medical grade 23 Ti6Al4V ELI alloy was used in the form of spherical metal powder (AP&C, Boisbriand, Quebec, Canada), with particle size in the range of 10 – 45 µm. The implants were fabricated in the Additive Manufacturing Laboratory at the TU Delft (Delft, The Netherlands), using customized equipment (SLM-125, Realizer, Borchem, Germany).

The dimensions of the fabricated implants were 4 cm x 0.5 mm (length x diameter) and they presented 35.6 surface-to-volume ratio. Vacuum cleaning and a three-step sonication process (5 minutes in acetone, 96% ethanol and demineralized water consecutively) were employed after the printing to remove loose particles.

2.1.2 Synthesis of strontium releasing surfaces

Strontium releasing surfaces were generated using plasma electrolytic oxidation setup consisting of AC power supply (50Hz, type ACS 1500, ET Power Systems Ltd., Chesterfield, United Kingdom) and computer interface connected with the power supply through a data acquisition board (SCXI, National Instruments, Austin, Texas, United States). A double-walled glass cell with a continuous supply of a cooling liquid was employed, enabling cooling of the electrolyte during the experiment. The implant was attached to a metallic holder with a crocodile clipper and secured with a waterproof tape. The reaction was performed in 800 ml electrolyte containing 0.15 M calcium acetate hydrate (Sigma Aldrich, USA), 0.02 M calcium glycerophosphate (ISALTIS, France), and in cases of strontium enriched implants 1 M strontium acetate (Sigma Aldrich, USA) at a constant stirring rate of 500 rpm, generating two kinds of surfaces (PT and PT-Sr respectively). At the start of each experiment, the temperature of the electrolyte was between 5 - 8°C. The sample was then immersed in the electrolyte in the middle of the electrolytic cell and connected to the electric circuit against a ring-shaped stainless-steel cathode. The plasma electrolytic oxidation was performed under galvanostatic conditions at two different current densities 20 A/dm^2 and 30 A/dm^2. The specimens were oxidized for 60, 90, 120, 180 and 300 seconds, to determine the effect of the oxidation time on surface topography. The changes in voltage were recorded at a sampling rate of 1/s. After completing the treatment, samples were cleaned with running water, rinsed with demineralized water, dried and cut into pieces of 1.0 cm length.

2.1.3 Assessment of surface morphology and chemical composition

The morphology of the synthetized surfaces was assessed by scanning electron microscopy. The implants were mounted onto the sample holder using a double-sided carbon tape. To generate a conductive layer and ensure visualization in the microscope, they were gold sputtered for 18 seconds (JEOL JFC-1300 Auto Fine Coater, JEOL USA) and placed in a JOEL scanning electron microscope (JSM-IT100, JEOL, Tokyo, Japan). Secondary (SED) and backscattered (BED) electron detectors were used at

low vacuum and 10 kV electron acceleration voltage for visualisation of the obtained morphology. The probe current was set to 50. Energy dispersive spectroscopy (EDS) was employed for analysis of the chemical composition.

2.1.4 Ion release profile

The Ca and Sr ions released from the surfaces were quantified through monitoring of the released ions throughout defined period of time. The 1 cm implants were inserted in 1.5 ml dark Eppendorf tubes (n = 3) with 1 ml phosphate-buffered saline (PBS) and incubated in a water bath at 37°C. The samples were removed from the tubes after 12 hours, 1, 4, 7, 14 and 28 days and transferred to a new set of tubes containing 1 ml PBS for the following time point. The cumulative number of ions released in the PBS solution at the defined time points was evaluated using inductively coupled plasma optical emission spectroscopy (ICP-OES).

2.1.5 X-ray diffraction

The phase composition of the PEO treated surfaces was determined through X-ray diffraction (XRD) method. The samples were fixed on a Si510 zero-background wafer in a standard L40 PMMA sample holder and placed in a BrukerD8 Advance diffractometer with Bragg-Brentano geometry and Lynxeye position sensitive detector (LL 0.19 W 0.05), Cu Kα radiation and divergence slit V6. The following settings were applied for the measurement: Coupled θ - 2θ scan in the range of 5° - 80°, a 2-second counting time per step and step size 0.008° 2θ. Bruker software DiffracSuite.EVA version 5.2 was used for evaluation of the data.

2.1.6 Sterilization of implants

Prior to *in vitro* tests, the implants were sterilized in a three-step process. First, they were immersed in 70% ethanol and sonicated for 3 minutes. They were then transferred and left in demineralized water for 5 minutes and finally sonicated for 30 seconds. Cleaned implants were dried, placed in a glass container covered with aluminium foil and sterilized in an oven at 125°C for 2 hours.

2.2 *In vitro* assays

2.2.1 Cell culture

For the *in vitro* tests, primary human umbilical vein endothelial cells (HUVECs) were used (catalogue number C2517A; single donor, Lonza, Switzerland). The cells were cultured in commercial EGM-2 media (Endothelial Cell Basal Medium-2, Lonza, Switzerland) containing several growth factors such as vascular endothelial growth factor (VEGF), recombinant human fibroblast growth factor (rhFGF), recombinant human epidermal growth factor (rhEGF), and others. All precultures for experiments were started as passage 5.

Prior to every experiment and for expansion purposes, HUVECs were precultured in flasks at a density of 2,500 cells/cm^2 in EGM-2 media at 37°C and normal oxygen level and refreshed with EGM-2 media three times per week. On day 7, cells were trypsinized, counted and seeded.

2.2.2 Seeding protocol

The sterile implants were transferred to 0.2 ml PCR Eppendorf tubes. Fibronectin bovine plasma (#F4759, Sigma Aldrich, USA) solution was added to each tube (100 µl of 0.05 mg/ml) to coat the

implants with the protein. The implants were then incubated with fibronectin at room temperature for 45 minutes. Immediately after, they were transferred to clean tubes and 150 µl of cell suspension containing 100,000 cells was added. The implants were then incubated in the tubes at 37°C for 2 hours and turned horizontally every 20 minutes to ensure uniform coverage of the implants. The implants were then taken out of the tubes and transferred in a 48-well plate with 200 µl of EGM-2 medium. The cells were cultured at 37°C and normal oxygen level and were refreshed with EGM-2 media three times per week.

2.2.3 Seeding efficiency

To determine the number of cells that attached onto the implant during the 2-hour seeding procedure, a seeding efficiency test was performed. After 2 hours of seeding, cells remaining in the tubes after removal of the implant were counted by mixing 10 µl of the cell suspension with 10 µl of Trypan Blue Dye 0.4% solution (Bio Bio-Rad Laboratories, USA). 10 µl of the mixture was then pipetted into the counting chamber and counted on a TC20™ Automated Cell Counter (Bio-Rad Laboratories, USA). The cell count was obtained as an average of two measurement per one sample. The seeding efficiency was calculated as a ratio of the remaining cells and the cells seeded initially in the tube.

2.2.4 Trypsinization

Wells with/without implants were washed twice with PBS and implants were transferred to 0.5 ml Eppendorf tubes. 50 µl of trypsin (Lonza, Switzerland) was added to each well of a 48-well plate and 100 µl of trypsin (Lonza, Switzerland) was added to each tube and the samples were incubated for 5 minutes at 37°C. Finally, 200 µl and 400 µl of medium was added to the wells and tubes, respectively, to deactivate the trypsin, and the implants were removed from the cell suspension.

2.2.5 Cell morphology

Cells were cultured on the implants with and without strontium at the seeding density of 100,000 cells per implant for 4 and 7 days. After each timepoint, the cells were washed with phosphate buffered solution (PBS), fixed with 4% paraformaldehyde (PFA) + 1% glutaraldehyde (GA) in PBS (PBS; pH 7.4) for 15 minutes and then washed twice with demi-water. The plates were then either stored in demi-water at 4°C for up to one week or directly dehydrated. For dehydration, cells were washed with demi water for (2 x 5 minutes), 50% ethanol (15 minutes), 70% ethanol (20 minutes) and 96% ethanol (20 minutes) to remove the moisture. The ethanol was then removed from the samples and they were left to air-dry for at least two hours. The samples were gold sputtered for 30 seconds (JEOL JFC-1300 Auto Fine Coater, JEOL USA) and morphology was imaged using a scanning electron microscope (JSM-IT100, JEOL, Tokyo, Japan) with the same protocol as described in section 2.1.3.

2.2.6 Presto Blue metabolic assay

Implants with/without strontium seeded with HUVECs were cultured for 1, 4 and 7 days. At each timepoint, the implants were transferred to a new well of a 48-well plate with 180 µl of EGM-2 media and 20 µl of Presto Blue staining solution (Presto blue, #A13262, Thermo Fisher, USA). Following 60 minutes of incubation, 100 µl of media with the staining solution was pipetted in a 96-well plate and the metabolic activity of cells was measured at an excitation wavelength of 535 nm and emission wavelength of 590 nm using a VICTOR X3 Multilabel Plate Reader (Perkin Elmer, USA).

2.2.7 EdU proliferation assay

A Click-iT™ EdU Cell Proliferation Kit for Imaging (Invitrogen™ Molecular Probes™, Thermo Fisher Scientific, USA) was used for this assay. Implants with/without strontium seeded with HUVECs were cultured in a 48-well plate for 2, 4 and 7 days. As control, HUVECs at a density of 10,000 cells/well were cultured in the same plate. Prior to each timepoint, 10 mM EdU was added to the EGM-2 medium. After 24 hours incubation, the wells with implants were washed with PBS, trypsinized and transferred to 1.5 ml Eppendorf tubes. The tubes were then centrifuged at 400 rcf for 5 minutes, and the supernatant was replaced with 100 µl of 1% BSA in PBS (PBS/BSA) and centrifuged. The supernatant was exchanged with 10 µl of fixative (component D). After 15 minutes of incubation (at room temperature and in the dark), 100 µl of PBS/BSA was added and the tubes were centrifuged. The supernatant was removed and 10 µl of permeabilization component (component E diluted 1:10 in PBS/BSA) was added. After an incubation for 30 minutes at room temperature, 100 µl of PBS/BSA was added to the pellet. The tubes were centrifuged, and the supernatant was replaced with 75 µl of Click-it reaction mix (624.15 µl PBS/BSA, 14.25 µl $CuSO_4$, 3.56 µl Alexa Fluor™ 488, 71.25 µl a diluted component G (1:10). The pellets were incubated for 30 minutes, 100 µl of PBS/BSA was added and the tubes were centrifuged. The supernatant was then replaced with 50 µl of PBS/BSA and the samples were run on a fluorescence activated cell sorting (FACS) machine (BD Accuri™ C6 Flow Cytometer, BD Biosciences, USA). The obtained results were gated accordingly, and the percentage of actively proliferating cells were compared.

2.2.8 Enzyme-linked immunosorbent assay (ELISA)

HUVECs were cultured under different conditions and refreshed 24 hours prior to collection of supernatants on day 2, 4 and 7. The media obtained from the cells were then centrifuged at 2,000 rcf for 10 minutes to remove the cell debris. Samples were either stored at -20°C or directly proceeded with next steps.

For the analysis, Human VEGF and Human FGF-21 Simple Step ELISA® Kits (Abcam, catalogue number ab222510 and ab222506) were used. Seven standards were prepared by reconstituting the respective lyophilized protein with a diluent provided in the kit and creating seven serial dilutions. A tube containing only the diluent and no protein served as a blank control. Standards were then pipetted in duplicates into the 96-well plate in a volume of 50 µl. Two-fold dilutions of all samples were created by pipetting 25 µl of a supernatant and 25 µl of the diluent into the plate. Antibody cocktail (containing Capture Antibody, Detector Antibody and Antibody Diluent) was then added to each well in a volume of 50 µl. The plate was sealed and placed on a plate shaker at 400 rpm and 20°C for 1 hour to ensure proper but gentle mixing of the solutions. Wells were then thoroughly washed with 3 X 350 µl of Wash Buffer PT (provided in the kit), to remove any remaining supernatant and antibody cocktail. 100 µl of a TMB Solution was then pipetted to each well and the plate was incubated in the dark on a plate shaker for 10 minutes (400 rpm, 20°C). Finally, 100 µl of a Stop Solution was added to the plate and the OD was read at 450 nm on a VICTOR X3 Multilabel Plate Reader (Perkin Elmer, USA).

The OD of the blank was subtracted from every value. The standard protein concentrations were plotted against the respective OD values, creating a standard curve. The protein concentrations of all other samples were obtained by interpolating those values to the standard curve.

2.2.9 Wound healing assay

Implants with/without strontium were seeded with HUVECs and placed in 12-well transwell inserts (one implant/transwell) with 0.4 µm pore diameter (w_cells). The wells of the 12-well plate were seeded with 80,000 cells/well. To relate the concentration of ions released from the implant surface to that of a flat surface, each transwell contained 4 implants in the end (one seeded with cells and 3 without cells). Another plate, containing 4 implants without cells in each transwell, served as a control of the paracrine effect between cells seeded on the implants and cells on the bottom of the well plate (wo_cells). The plate layout for each experimental group is illustrated in Figure 1. The volumes of EGM-2 media added to the transwell and 12-well plate, were 400 and 700 µl, respectively. The plates were incubated for 3 days until confluence in the wells was reached. The plates were then refreshed with EGM-2 medium deprived of serum and subjected to a 24-hour serum starvation to synchronize the cell cycle. To create a wound, the confluent layer was scratched using a 200 µl pipet tip and washed twice with PBS to remove the debris. The plates were replenished with EGM-2 medium. Pictures of the scratches were taken at 0, 13, 16, 19, 22 and 48 hours post-scratching using a ZOE Fluorescent Cell Imager (Bio-Rad Laboratories, USA). The scratches were analysed by measuring the remaining width at 2 locations along the scratch (4 measurements per location).

2.2.10 Coculture of HUVECs with conditioned medium from MSCs

To investigate the paracrine effect of mesenchymal stromal cells on angiogenic behaviour of endothelial cells, HUVECs were cultured in the presence of conditioned media (CM) obtained from MSCs exposed or not to strontium. MSCs (passage 7, donor 4266, Lonza, Switzerland) were precultured with Lonza Mesenchymal Stem Cell Medium, and then seeded in T75 flasks at a density of 7.5×10^5 cells per flask. The cells were cultured at 37°C, 5% CO_2 and normal oxygen levels and refreshed with 10 ml of

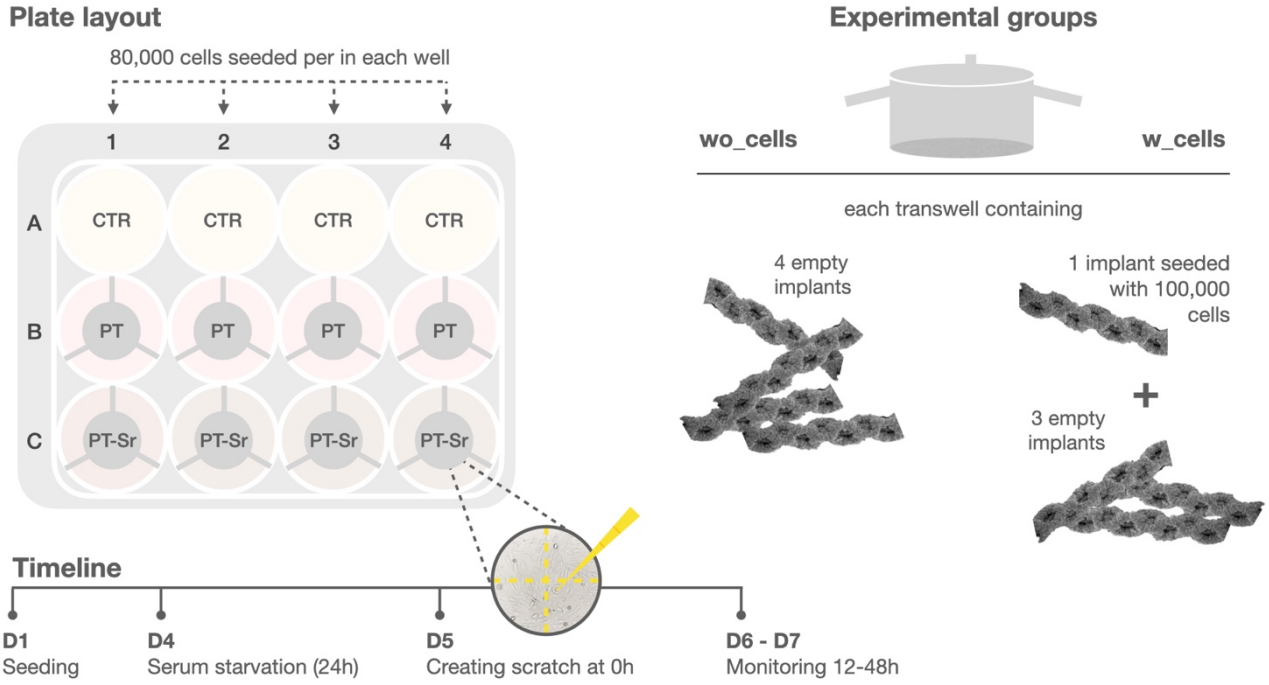

Figure 1. An illustration of the experimental setup for the wound healing assay. Two experimental groups, w_cells (transwells containing 1 seeded implant and 3 empty implants) and wo_cells (transwells containing 4 empty implants), were compared. Each group was studied in a separate plate containing 3 experimental conditions: control (CTR), PT, PT-Sr.

10% αMEM (containing 10% FCS, 20 ml/l Pen/strep, 20 mM HEPES, 1.8 mM $CaCl_2 \cdot 2H_2O$, as described in [41]) on day 2, 5 and 7. On day 9, αMEM with 0.1% BSA and with (CM-Sr) and without (CM) 0.3 mM strontium acetate (SrA) was added to the cells and the flasks were transferred to a 3% O_2 hypoxic incubator for 48 hours. On day 11, the conditioned medium (CM and CM-Sr) was collected, 2% of serum was added, and the medium was filtered and aliquoted.

HUVECs were seeded on PT and PT-Sr implants at the normal seeding density described in section 2.2.2 and the implants were placed in 48-well plates. EGM-2 and CM/CM-Sr were mixed in a 1:1 ratio and an aliquot of 200 µl was added to each well. A plate containing only EGM-2 medium served as control. The overview of the experimental groups is presented in the Figure 2.

The effect of the different conditions on the angiogenic capacity of HUVECs after 4 days of culture was assessed through ELISA (described in section 2.2.8), which quantified the secretion of VEGF and FGF21 by measuring the OD values on a VICTOR X3 Multilabel Plate Reader (Perkin Elmer, USA).

2.3 Statistical analysis

Calculations were done in MATLAB and the obtained data were plotted using GraphPad Prism 8.0 (GraphPad Software, USA). The plots represent mean value ± standard deviation. The statistical significance of the data was evaluated using one-way ANOVA tests, with Bonferroni correction. Results were considered statistically significant when the $p < 0.05$.

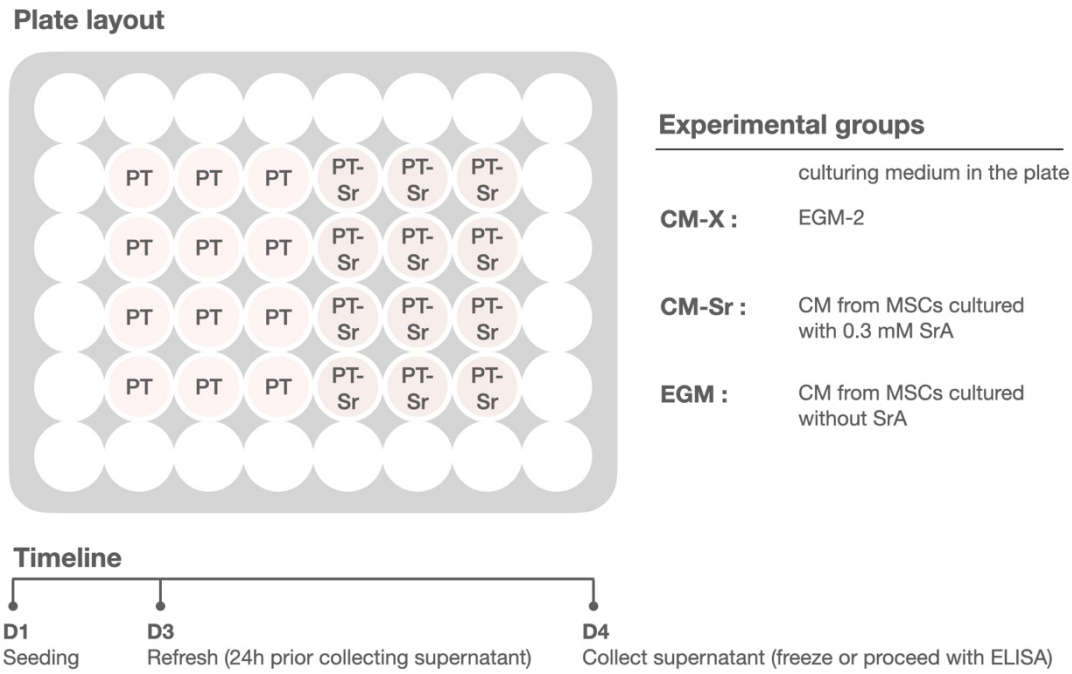

Figure 2. Illustration of the experimental setup for the coculture experiment. Total of 3 plats were used for this experiment, each plate contained PT and PT-Sr conditions and was cultured with one of the 3 mediums (CM-X, CM-Sr, EGM). Medium from 3 wells was pulled together for each replicate, yielding 4 replicates per each condition.

3 Results:

3.1 Surface modification of implants and characterization of strontium releasing surfaces

3.1.1 Selection of optimal PEO parameters

In order to generate surfaces with strontium (PT-Sr) and control samples without strontium (PT), two electrolytes of different compositions were employed. The final PEO parameters for each condition were chosen after a set of optimization runs, with the aim to achieve the same topography on both PT and PT-Sr implants. In addition, the concentration of the strontium acetate added to the electrolyte had to be optimized to achieve a concentration of released Sr ions from the treated surfaces in the range previously shown in literature to positively influence HUVECs functions.

Thus, for PT-Sr implants, a current density of 30 A/dm^2 applied for 300 seconds was selected, and an electrolyte containing 0.15 M calcium acetate, 0.02 M calcium glycerophosphate, and 1 M strontium acetate was used. These parameters resulted in generation of strontium containing surfaces, which demonstrated ion release profile properties in accordance with findings from a conducted literature study, reporting a positive effect of strontium on angiogenic behaviour of HUVECs. For PT samples, a current density of 20 A/dm^2 and different PEO times of 60, 90, 120, 180 and 300 seconds were tested in an attempt to reproduce the topography of the PT-Sr implants. The images of the obtained surfaces are depicted in Figure 3 and show a topographical analogy between PT-Sr sample subjected to PEO under the above-described conditions (Figure 3A) and PT sample exposed to the PEO for 60 seconds

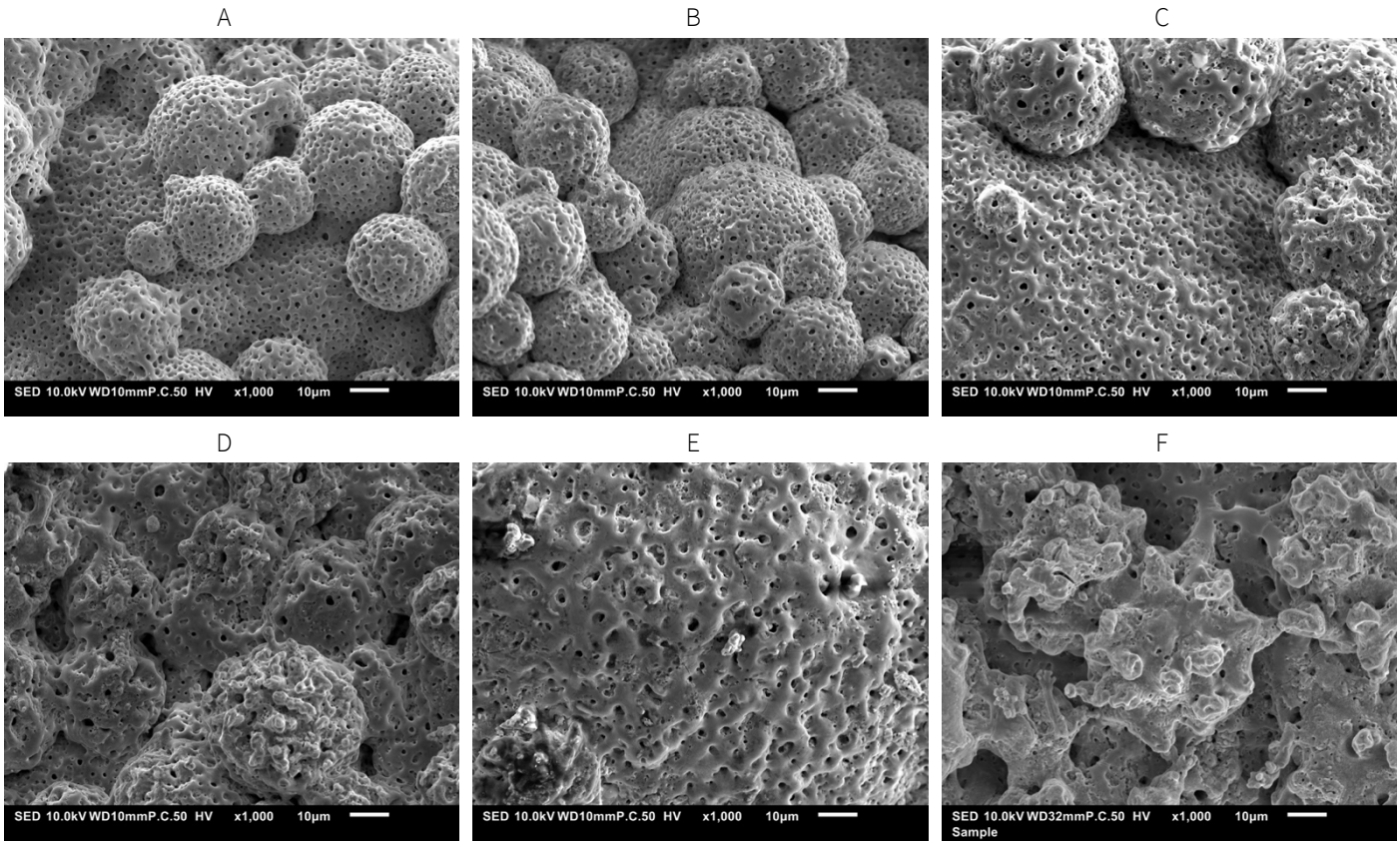

Figure 3. SEM images depicting the changing in surface topography of the implants with varying PEO parameters: A) PT-Sr sample treated under above-described conditions for 300 seconds, and PT samples after B) 60, C) 90, D) 120, E) 180 and F) 300 seconds of PEO.

(Figure 3B). When the PEO process was applied for 60 seconds, the partially melted metal particles left behind after the 3D printing process have preserved their integrity, suggesting generation of a thin oxide layer with uniformly distributed small pores. With prolonged oxidation (Figure 3C-F), the integrity of the metal particles was disturbed. The gradual growth of the oxide layer in the presence of larger plasma discharges occurring on the surface resulted in surface with larger pores and of greater roughness. After 300 seconds, the particles were hardly recognizable, and the pore size distribution has lost its homogeneity. Therefore, the PEO time for the surface treatment of PT samples used for further experiments was set to 60 seconds.

3.1.2 Assessment of morphology and phase composition

The comparison of the non-treated implant (NT) and topographies generated after the selection of optimal PT and PT-Sr conditions described in section 3.1.1 is captured in Figure 4. Obtaining analogous surface morphology on both samples was a necessary prerequisite for later *in vitro* tests. Surface topography is a known cue used for stimulation of cellular response and its variability among the two

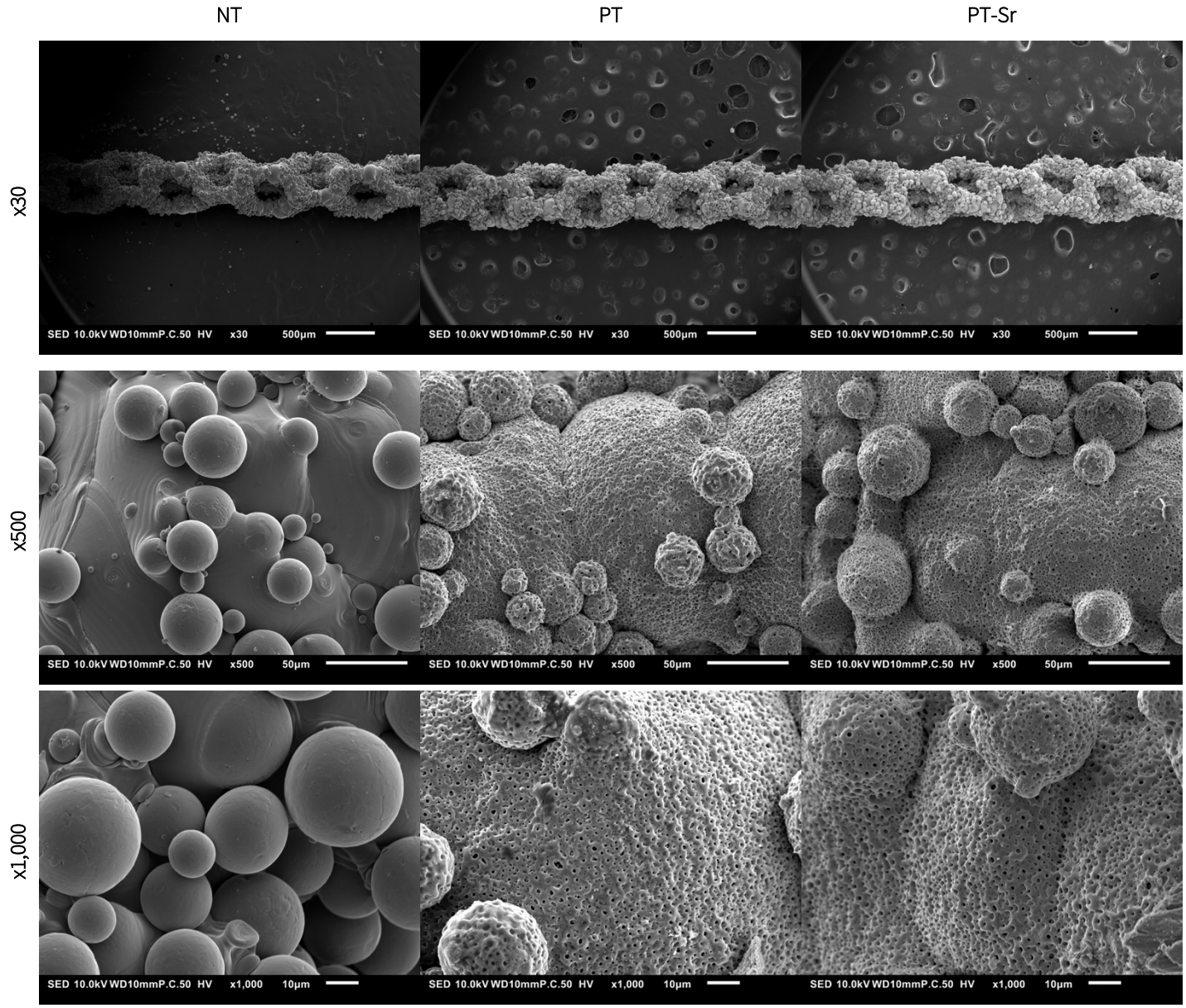

Figure 4. Morphology of implants before (NT) and after PEO treatment in electrolytes without (PT) and with (PT-Sr) strontium, at different magnifications (x30, x500, x1,000).

samples would introduce an additional variable into the assessment of strontium effects on HUVECs. The biofunctionalized samples utilized for the angiogenic assays demonstrated surfaces with microroughness, attributed to the residual particles from the 3D printing process, and fine pores structures, generated during the electrochemical treatment.

The phase composition of the synthetized surfaces was assessed with X-ray diffraction (XRD) and the diffraction spectra are in Figure 5. It revealed presence of the crystalline TiO_2 in the form of its two polymorphs anatase and rutile, on both PT and PT-Sr implants. The occurrence of these two phases appeared to be relatively balanced on the PT samples while PT-Sr implants demonstrated greater content of the rutile phase. This could be attributed to the conditions of the PT-Sr reaction (longer exposure and possibly higher temperature), which would favour the establishment of the high temperature rutile phase over low temperature anatase. Strontium was found in the form of strontium titanate ($SrTiO_3$) and strontium oxide phosphate ($Sr_{10}O(PO_4)$) on the PT-Sr samples, the latter being a strontium analogue of hydroxyapatite ($Ca_{10}(PO_4)_6(OH)_2$).

3.1.3 Ion release profile

In order to quantify the level of bioactivity of the PEO treated surfaces due to ions released, analysis of Ca^{2+} and Sr^{2+} ions (Figure 6) released from the surfaces of PT and PT-Sr samples in PBS was performed

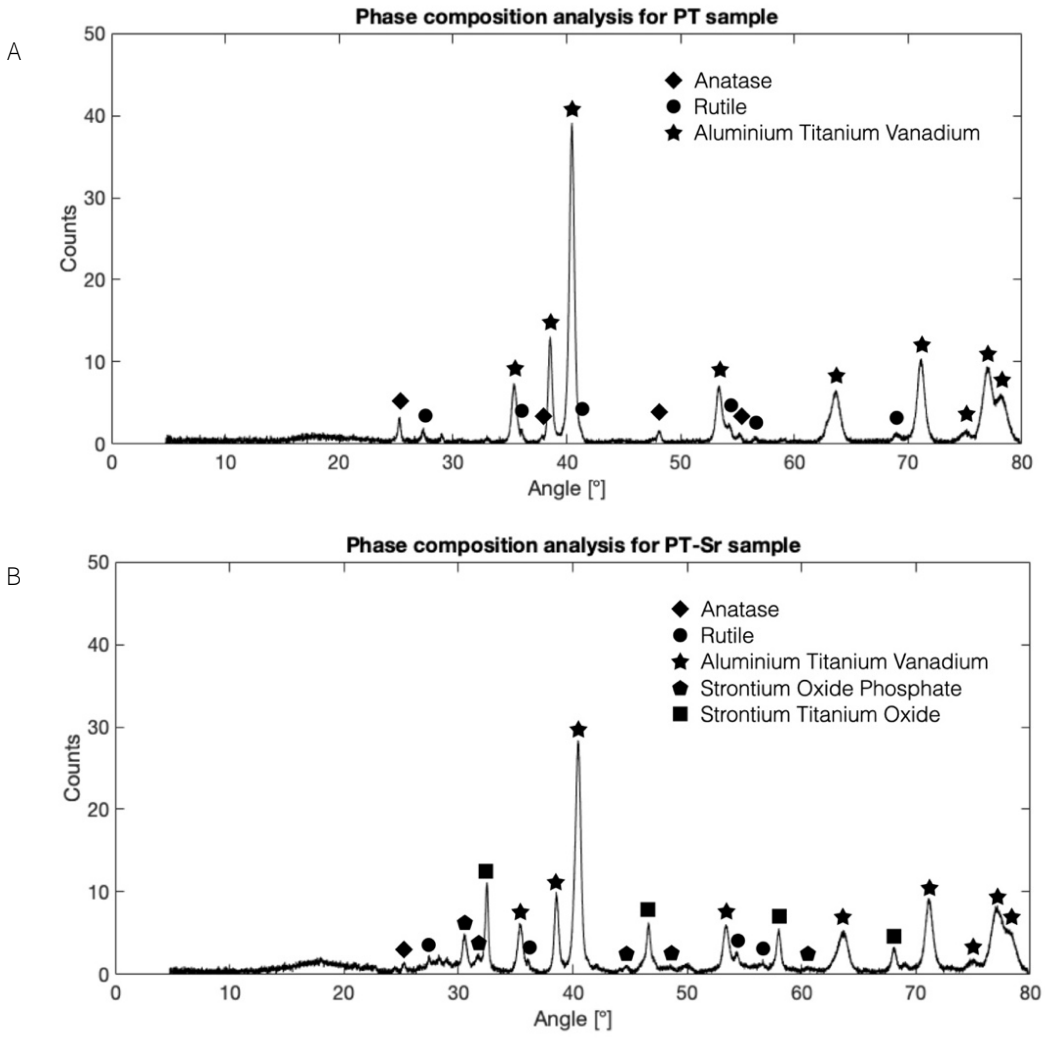

Figure 5. Results of the XRD analysis performed on the A) PT and B) PT-Sr samples depicting the phase composition of the PEO synthetized surfaces.

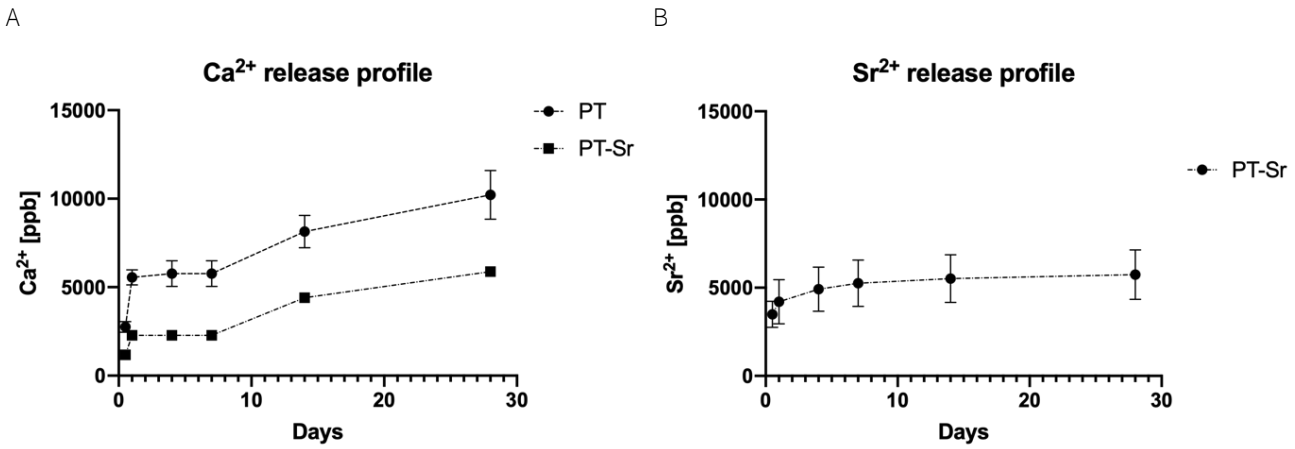

Figure 6. Results of the ICP-OES analysis depicting the ions release profiles of A) calcium and B) strontium from the surfaces of PT and PT-Sr samples in PBS over a period of 30 days.

over a period of 30 days. The calcium ion release maintained the same trend in both PT and PT-Sr samples. Their profile demonstrated high release rates in during the first 24 hours, while flattening in the first week, and followed by a gentle incremental ion increase throughout the next 3 weeks. The maximum amount of detected Ca^{2+} after 28 days was 10,213 ppb in PT and 5,877 ppb in PT-Sr samples. The release of strontium detected in PT-Sr samples was lower in comparison to the released calcium ions. The initial steep release occurred within the first 3 days, after which the profile reached a plateau and maintained it throughout the rest of the monitored period. The amount of detected Sr^{2+} after 28 days reached 5,742 ppb.

3.2 Effect of the PEO treated surfaces on the behaviour of HUVECs

3.2.1 Seeding efficiency of HUVECs on PEO treated surfaces

Different seeding protocols were tested to determine the most efficient approach for seeding of HUVECs onto the PT and PT-Sr implants. A cell density of 100,000 cells per implant was used and the implants were incubated for 1 or 2 hours and turned every 10 and 20 minutes, respectively. Moreover, the effect of an additional fibronectin coating was tested.

The results (Figure 7) revealed that implants with fibronectin coating incubated for two hours exhibited the highest seeding efficiency of 90% and 92% for PT and PT-Sr samples respectively. Seeding protocol with fibronectin and incubation of one hour yielded efficiency of over 80%, suggesting that the majority of cells attach within the first hour and that excessively prolonged incubations do not further increase the seeding efficiency. In contrast to that, a trend of lower seeding efficiency with greater standard deviation was observed on implants without the fibronectin coating.

The final seeding protocol applied for further assays included fibronectin coating and incubation of 2 hours before transferring implants to the well plates for further culture.

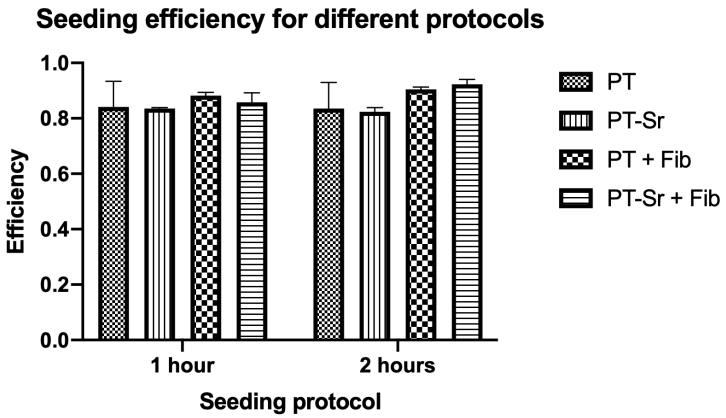

Figure 7. Comparison of seeding efficiency on PT and PT-Sr implants with/without fibronectin and incubation length of one or two hours.

3.2.2 Effect of implant surfaces on attachment and morphology of HUVECs

The implants were subjected to incubation with cells for several days to assess the long-term attachment of HUVECs on the surfaces with/without the fibronectin coating. The implants incubated with cells for 4 and 7 days were imaged in SEM. The qualitative assessment conducted through SEM imaging (Figure 8) revealed that implants without the protein coating presented a decreasing trend in number of cells found on the implant surfaces, implying that cells fell off/left the implants during the period of 7 days. Many cells were seen settled on the bottom of the wells already on day 4 after seeding, where they continued to proliferate in the proximity of the implant. The metabolic activity of these cells was assessed with a Presto Blue assay on day 1, 4 and 7 after seeding and the obtained data complied with the previously mentioned observations presuming detachment of HUVECs from the implants (Figure 9). On day 4, the fluorescence values were slightly lower for cells in the wells, indicating less cumulative metabolic activity of the well, in comparison to cells on the implants (Figure 9A). This trend, however, reversed over the next 3 days, resulting in much higher cellular activity detected in the wells compared to the implants on day 7. A comparable trend was observed for both experimental conditions (PT and PT-Sr implants) with no difference in metabolic activity between the two groups at any of the defined time points. The cellular activity increased for both groups in the first few days, with a peak on day 4, followed by a decline detected on day 7 (Figure 9B).

In contrast to that, the presence of fibronectin seemed to secure a stronger long-term attachment of HUVECs even after 4 and 7 days and thereby could promote a further coverage of the samples by those cells. Although there was no apparent observable increase in the number of cells incubated on surfaces equipped with fibronectin between day 4 and 7, they seemed to gradually adopt a greater spread in comparison to samples lacking the protein. However, even with the coating, some cells were still found on the bottom of the wells, surrounding the PT and PT-Sr implants.

The images also depicted the variability of the implant topography and its effect on the coverage of its surface by HUVECs. Noticeably more cells were found in the macropores (attributed to the design of the implant) in between the partially molten metal particles, which seemed to provide a favourable structural anchorage for HUVECs, than on the “smooth”/flat regions deprived of such structural features. Overall, no differences in the behaviour of cells seeded on the surfaces of PT versus PT-Sr implants were observed.

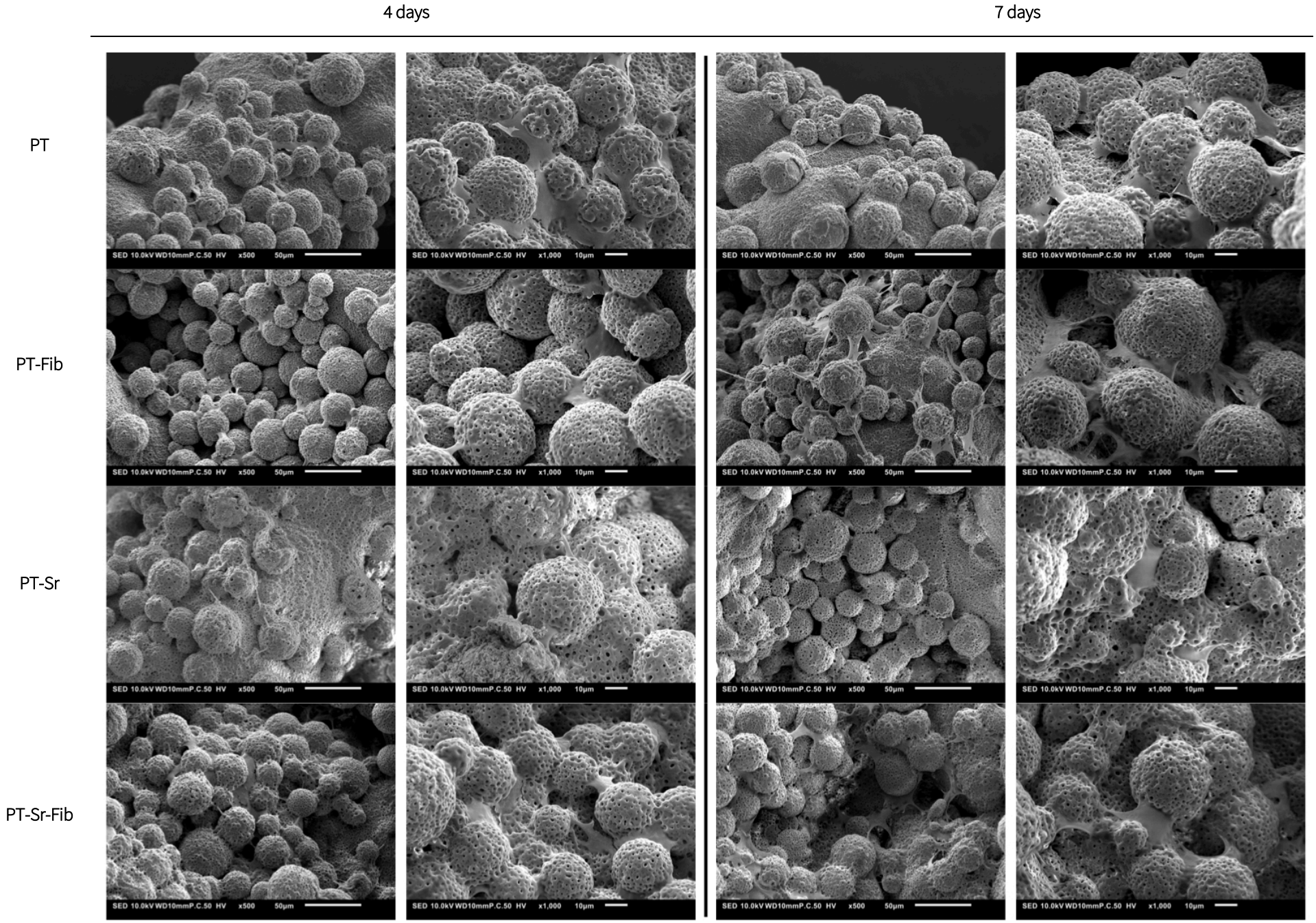

Figure 8. *SEM images of HUVECs seeded on PT and PT-Sr implants with and without fibronectin coating. Cells were incubated for 4 and 7 days.*

A

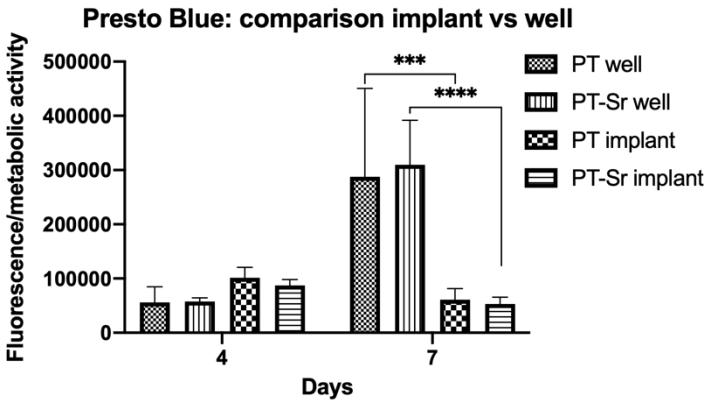

B

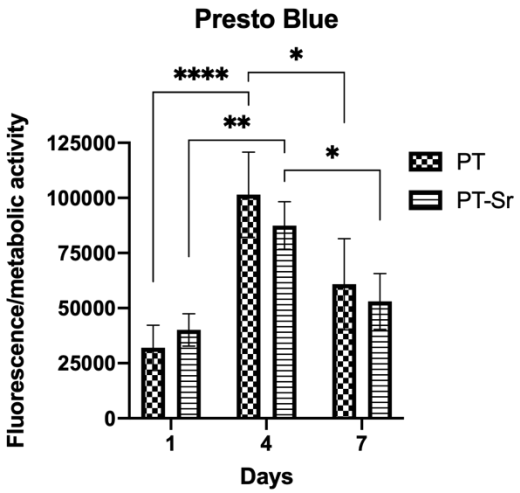

Figure 9. Presto Blue depicting the differences in metabolic activity of cells seeded on the PT and PT-Sr implants and cells found in the wells after incubation of 4 and 7 days.

3.2.3 Proliferation of HUVECs on the PEO treated surfaces

The proliferative response of HUVECs to PT and PT-Sr implants was investigated through an EdU proliferation assay. The obtained results are shown in Figure 10A. The rate of actively proliferating HUVECs seeded on PT and PT-Sr samples was found to be in the range of 40 – 65% throughout the monitored time period (2, 4, and 7 days after seeding). The detected proliferative activity in the three experimental conditions (Control, PT, PT-Sr) followed a similar trend at all time points, with the highest values being reached on the second day. On day 4, cells on PT implants exhibited higher proliferative activity than cells on PT-Sr surfaces. No differences were, however, observed at the other timepoints, suggesting that the chemical composition of the two tested bioactive surfaces (PT and PT-Sr) does not strongly influence the proliferation of HUVECs. Moreover, the effects of the PT and PT-Sr surfaces did not vary from the control (cells seeded in wells), suggesting that the strontium surfaces do not impede the endothelial proliferation.

ELISAs were performed to quantify the release of VEGF and FGF-21 by HUVECs on day 2, 4 and 7 of culture (for more information about those growth factors, refer to Appendix 8.4.3). PT and PT-Sr samples exhibited akin characteristics with respect to the FGF-21 and VEGF secretion by HUVECs (Figure 10B and C). Relating the obtained results to the EdU data showed some correlation between the proliferative rate and the FGF-21 levels. Clear interpretation, however, was complicated by the relatively large error of ELISA replicates (especially for VEGF).

3.2.4 Effect of the PEO treated surfaces on wound healing

The healing capacity of HUVECs was assessed in a wound healing assay (sometimes also referred to as scratch assay). In addition to the effect of ions released from the bioactive surfaces of the implants, this set up and the selection of experimental groups intended to test also the effect of paracrine signalling occurring between cells seeded on the implants (and placed in transwells) and cells seeded directly in the wells, on wound healing.

The quantitative interpretation of the wound closure (in the bar chart in Figure 11) depicts the changes in the wound width obtained from measurements carried out at 0 hours and then every 3 hours between 12 and 21 hours. The cells seem to be more active throughout the first 12 hours, managing to

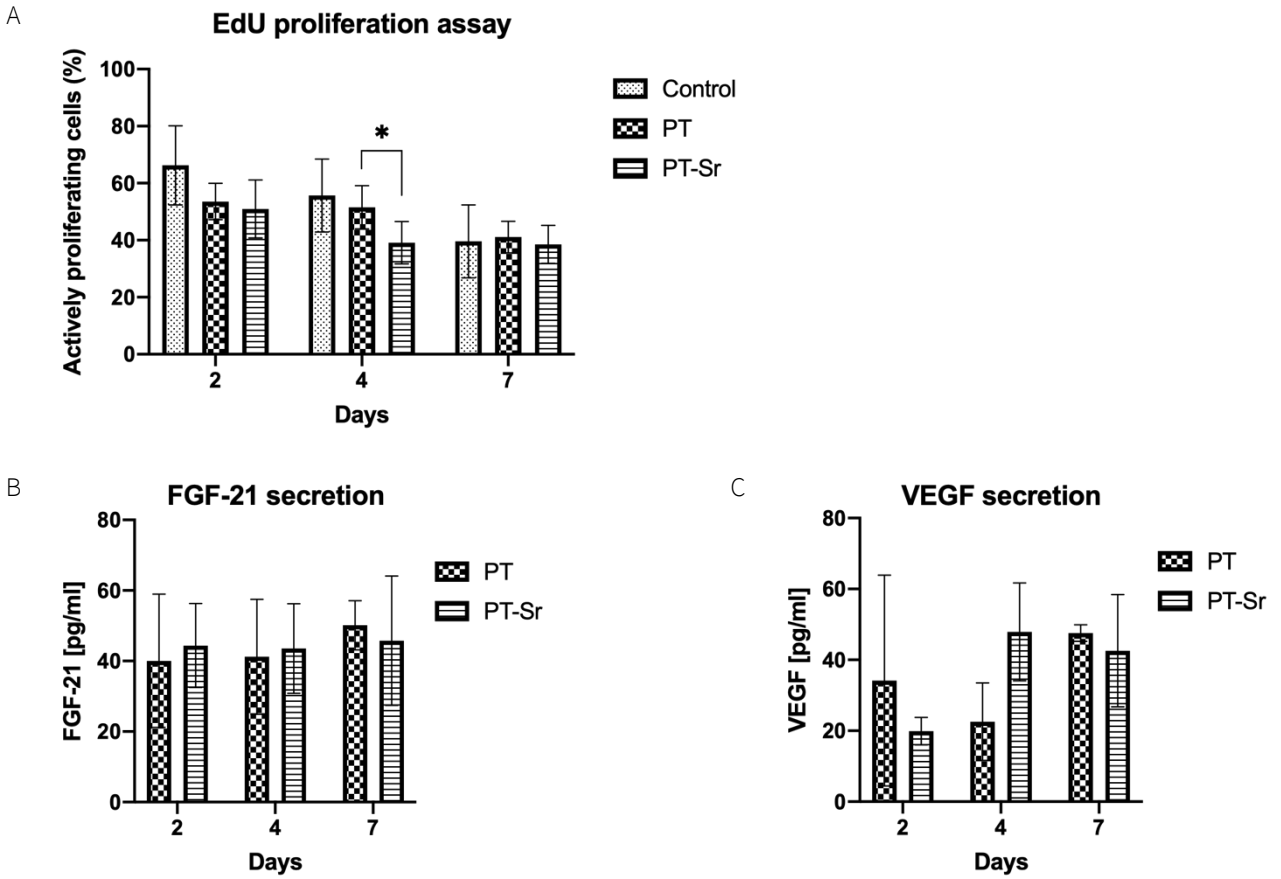

Figure 10. Assessment of actively proliferating cells through A) EdU assay on days 2, 4 and 7 after seeding, and the expression of B) FGF-21 and C) VEGF as a recorded response of HUVECs to the different implant surfaces on day 2, 4 and 7.

close nearly 40 - 50% of the wound, while their healing efficiency decreased between 12 and 21 hours, healing the wounds to about 55 – 65%. After 48 hours, all wounds were fully closed. The obtained data showed no difference between the healing capacity elicited by the ionic products from PT and PT-Sr samples alone (plate without cells). The results also imply that neither of the ionic products from PT and PT-Sr implants instigated paracrine communication between the cells on the implants and cells seeded in the wells, which would facilitate wound closure. All in all, a comparable decreasing trend among all experimental groups without any significant differences was observed.

Figure 12 contains images of confluent monolayers of HUVECs before creating a scratch, and images capturing the full width of a wound at 0 hours and a partially closed wound at 15 hours.

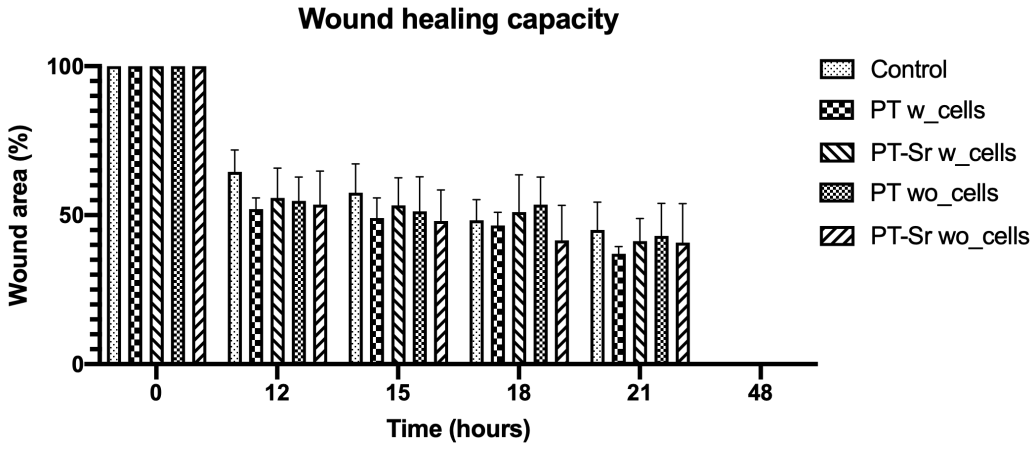

Figure 11. Wound healing capacity depicted as the portion of the wound area measured at different time points; scratches were made at 0 hours and counted as a reference (100%) for the following measurements.

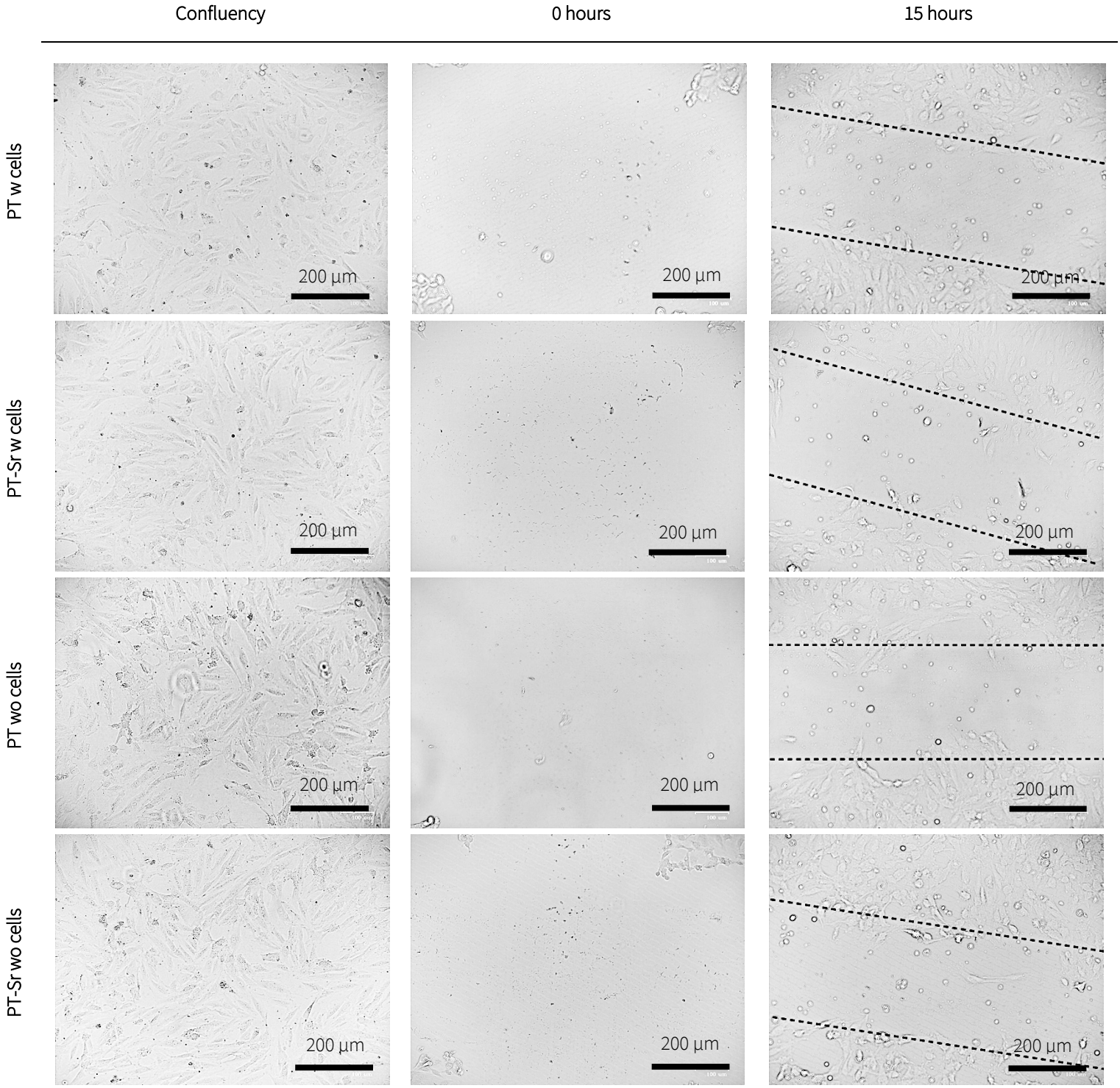

Figure 12. Images showing the confluency of cells, and wound area at 0 and 15 hours for the different experimental conditions.

3.2.5 Angiogenic capacity of the HUVECs and MSCs coculture system

To approximate the complex *in vivo* interactions occurring during the fracture healing process, HUVECs were cultured for 4 days in CM obtained from MSCs. MSCs were cultured in culture media with and without strontium. The subsequent effect of these conditions on HUVECs seeded on PEO modified surfaces was assessed by comparing concentrations of two angiogenesis-related proteins, VEGF and FGF-21, in three experimental groups, each containing different culturing media (CM-X, CM-Sr, EGM; section 2.2.10).

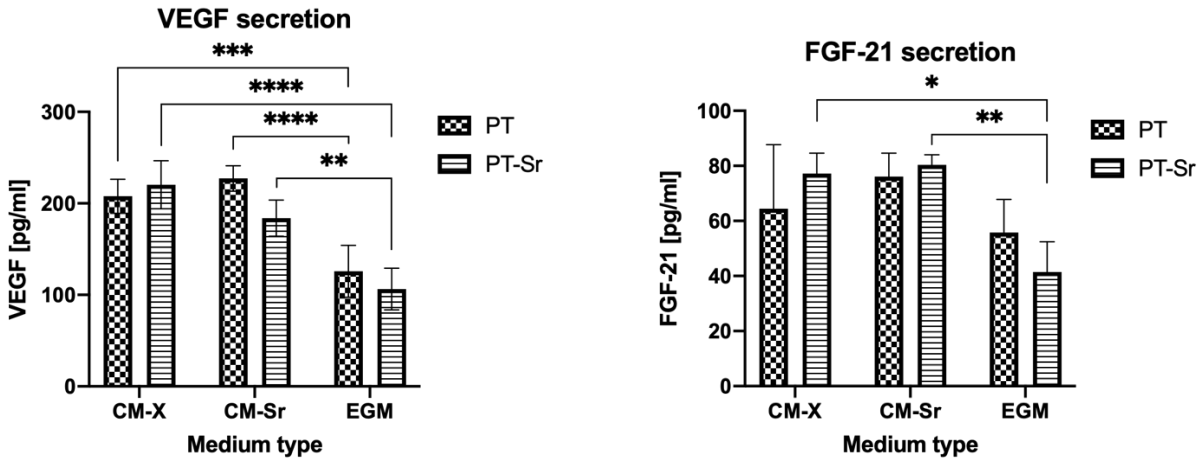

Figure 13. VEGF and FGF-21 concentration detected in the 3 experimental groups (CM-X, CM-Sr, EGM), each comprising of two conditions (PT and PT-Sr) after culturing HUVECs in the respective media for 4 days.

Figure 13 illustrates the results of the conducted ELISAs for VEGF and FGF-21 on the cocultures. The obtained data indicated that VEGF reached higher values in groups containing either of the two CM (CM-X and CM-Sr) in comparison to the EGM. The results for FGF-21 attained a similar trend of higher protein concentrations in the coculture systems than in EGM only, although a significant improvement was recorded only for PT-Sr condition. Neither of the three experimental groups demonstrated any distinct effects between the two types of surfaces (PT vs PT-Sr) and two types of CM (CM-X vs CM-Sr) on the VEGF and FGF-21 content in the media. VEGF was found to be expressed at higher levels (about 2 - 3 fold) in comparison to FGF-21. These findings showed that a coculture system comprising of MSCs (or their CM) and HUVECs presented higher concentrations of VEGF and FGF-21 and thereby could offer beneficial proangiogenic stimuli and promote the angiogenic commitment of HUVECs.

4 Discussion

Aseptic loosening is recognized as one of the leading causes of implant failure after primary THA. Incorporation of angiogenesis and osteogenesis boosting agents into the biomaterial's surface could strengthen the attachment at the bone-implant interface and very likely improve the failure odds. Strontium has been recognized as a strong promotor of bone formation and its robust osteoconductive character has been increasingly studied. This study addressed its potential role in the formation of vascularized bone by investigating its effects on the behaviour of endothelial cells. For its auspicious properties, combining this bioactive trace element with a suitable load bearing biomaterial could offer a solution that could effectively promote osseointegration and grant a more secure attachment between the bone and the implant.

4.1 Effect of PEO parameters on the surface properties of modified implants

Plasma electrolytic oxidation was employed for modification of the titanium implants. The implants were subjected to PEO treatment in two electrolytes with different composition and at different current densities, generating two types of surfaces (PT and PT-Sr) with comparable topographies and distinct chemical composition.

The PEO treatment generally results in generation of a relatively diverse spectrum of phases on the material's surface. The final phase composition is dependent on the bulk material subjected to the oxidation and the process parameters, such as electrolyte composition, oxidation time, applied current density or voltage. The higher occurrence of TiO_2 in the tetragonal rutile morphology on the PT-Sr samples can be attributed to the higher current density and oxidation time used for these implants, resulting in convenient transformation of thermodynamically metastable anatase into more stable rutile [42,43].

Hydroxyapatite, which comprises the inorganic component of bone crystals and its deposition on biomaterials surfaces has been shown to have beneficial effects on bone formation, was not detected on either of the two surfaces. The reason for its absence on PT samples may be the short PEO duration. According to a previous study performing PEO in an electrolyte of identical composition, first HA crystals were detected after 120 seconds [40]. Other PEO data obtained with electrolytes composed of calcium acetate and calcium glycerophosphate (exact concentration was not given) showed that HA started appearing on the surfaces only after 5 minutes and gradually became the major phase with prolonged duration of the reaction [43]. Strontium analogue of HA, $Sr_{10}O(PO_4)_6$, was detected on PT-Sr samples.

4.2 Response of HUVECs to the PEO treated implants

In this work, the response of HUVECs to the PEO treated 3D printed titanium implants was investigated. Previously conducted studies of those surfaces with preosteoblastic cells confirmed their osteogenic character while proposing a new fitting solution for load bearing orthopaedic implants [39,44] which could effectively promote osseointegration and thereby secure a stronger attachment between the biomaterial and the tissue. Considering the importance of blood vessel development in the early stages of fracture healing (section 8.3.1 in the Appendix), it was imperative to investigate the effects of those

surfaces on the behaviour of endothelial cells as a next step, to rule out any hindering/inhibitory effects on the development of a healthy vascularized bone.

The exact mechanism by which strontium activates ECs and guides their angiogenic behaviour is not yet fully known, however, the role of the calcium-sensing receptor (CaSR) has been speculated [25]. This receptor is inherently involved in the mechanism of strontium-facilitated osteogenesis. It can bind strontium instead of calcium due to its similar atomic and ionic properties [45,46]. Confirming the role of CaSR in the strontium-mediated angiogenic commitment of ECs would introduce a new and possibly very effective system for the early development of well-vascularized bone.

Despite the limited knowledge on the role of this element in vessel formation, data from the reviewed literature indicated favourable effects through enhanced endothelial activity and angiogenic stimulation/differentiation with Sr^{2+} in the range of 1 – 6.0 mg/l (cumulative ions release after 7 days) [23,28,47], which was in compliance with ion release profile of PT-Sr implants (6.7 mg/l Sr^{2+} after 7 days). The response of HUVECs to the strontium containing implants was evaluated through several assays, assessing their attachment, morphology, proliferation, wound healing ability and angiogenic potential/differentiation.

The topic of cell-biomaterial interactions has been widely investigated in the past and presently numerous physical and chemical cues are known to control viability and further thriving of cells. The first information about the compatibility of a biomaterial for adherent cells is the ability to sustain cell attachment. This initial response is determinative for any further interactions, as cells cannot proliferate and differentiate without attaining a proper anchorage [48,49]. The attachment of HUVECs during seeding on the PT and PT-Sr surfaces was satisfactory, reaching over 80%. The present knowledge about cellular adhesion strictly associates it with the degree of protein adsorption to the biomaterial's, which in turn can be facilitated by higher wettability and certain degree of surface roughness [49–52]. The surfaces tested in this study presented submicron porosity, generated during the PEO treatment. Such surfaces demonstrating submicron- and nanopatterns have been reported to favour the attachment of endothelial cells [50,52–55] by offering larger surface area with higher number of possible anchorage sites [48,49,51], promoting further their proliferation and other vital functions, such as NO production expression of angiogenic factors [48,50,53,56]. Excessively hydrophilic surfaces, on the other hand, were reported to be suboptimal for the attachment [57] and resulted in lesser proliferative rate [48] suggesting each system must represent a set of balanced parameters for maximizing the positive effects/outcomes.

Despite the good initial attachment demonstrated by high seeding efficiency of HUVECs on the implants, cells were found to either fell off or leave the implant over the monitored period. After 7 days, hardly any cells were found on the implant's surfaces, suggesting that they lacked satisfactory cues for long-term endothelial attachment and migration. To sustain the cell-biomaterial connection, fibronectin coating was added to the seeding protocol. This extracellular matrix protein is known to facilitate adherence of cells to many materials by increasing the number of points for focal adhesion sites. Development of a bond between fibronectin and adhesion receptors in the cellular membrane (integrins) [58] leads to activation of intracellular signalling pathways responsible for cellular viability, proliferation and further differentiation [59]. The coated implants retained higher number of cells even on day 4 and 7 after seeding, which was in line with findings in the literature [59].

Unlike MSCs [39], HUVECs tested in this study failed to establish a homogenous layer, even on the fibronectin coated surfaces, which is considered a prerequisite for endothelial sprouting preceding the formation of a vascular network [60,61]. Although the EdU assay and ELISA provided data confirming active proliferation of HUVECs on both PT and PT-Sr (with comparable results), the qualitative visual analysis of the implants in SEM did not substantiate an increase in number of cells on the surfaces between day 4 and 7. The images implicated that despite the active proliferation cells did not find enough of satisfactory cues to remain on the surfaces and many eventually left the implants. The fallen cells found on the bottom of the wells, however, continued to proliferate in the proximity of the implant, suggesting that the concentration of ions released from the surfaces does not reduce the viability of HUVECs.

Considering the complex characteristics of the PT and PT-Sr surfaces, it is unclear whether those undesirable effects are a result of the chemical composition or the physical properties of the implants. The ionic products from the implants did not show any facilitation in wound healing. The direct contact of HUVECs with PT and PT-Sr surfaces did neither elicit paracrine communication between the cells which would promote the closure of the created scratch, which is a result of a collective results of cellular proliferation and migration. These findings are inconsistent with previously reported data in the literature showing improved proliferation and migration (wound healing) properties of ECs cultured with extracts from strontium containing materials [23–28] or seeded directly on their surfaces [29,52] (in comparison to materials deprived of this element). However, it is imperative to account for possible exposure of cells seeded on the surfaces to other factors introduced by materials, which may also guide cellular responses (some of them were discussed earlier in this section). The anodized titanium foils used in [52] were presented with nanoporous structures and the researchers also reported the likelihood of those cues contributing to the enhanced endothelial activity. Varying surface topographies between tested biomaterials, which could substantially affect the ECs activity along with the chemical composition, were also reported in studies comparing the angiogenic properties of calcium-polyphosphate-doped with strontium (SCPP) and without (CPP). The SCPP presented larger and more interconnected pores, resulting in a smoother surface with greater amounts of Ca^{2+} and $(PO4)^{3-}$, which overall favoured the endothelial activity [29,30,62].

This hindrance in proliferation and migration may be possibly attributed to the microrough character of the surface, which in case of PT and PT-Sr implants is given by the manufacturing process. Surfaces of moderate roughness have been reported to be suboptimal for endothelial cells over more physiological smooth surfaces (smooth surfaces can still demonstrate submicron- and nanoroughness) [61,63]. The features on such surfaces, like residual particles on the surfaces of PT and PT-Sr implants, may represent obstructions for migration and proliferation of endothelial cells and impede cellular clustering and endothelial intercellular contacts [61]. These are absolutely essential/vital for angiogenesis, where stalk and tip cells migrate and proliferate together, creating sprouts which are then gradually rebuilt into new functional vasculature [60]. Therefore, despite higher expression levels of angiogenic markers on the rough surfaces, the proliferation and migration abilities of those ECs may be of lesser value [61]. This finding can be applied on the results of this study and justify their contradiction with findings in the literature reporting upregulated expression of angiogenic factors in the presence of strontium containing biomaterials [23,24,29].

All in all, neither of the PEO treated surfaces (PT and PT-Sr) did exhibit any superior effects on endothelial activity, however, no hindrances presented by either of those two materials were detected either. Another possible explanation for this endothelial behaviour could be an inadequate concentration of strontium ions released from the surface into the medium. A study employing a bioceramic material showed that even higher concentrations between 13-27 mg/l could favour the angiogenic behaviour of endothelial cells [64], while few other materials proved to be effective even at concentrations of less than 1 mg/l [21,24,30]. However, the vast majority of biomaterials investigated in these studies were very complex with multiple (bioactive) elements in their composition and their possible additive/synergistic effects should be taken into consideration. In this study, calcium was released from both implants with relatively close release rates. This intracellular element possesses a regulatory role in proliferation, migration and tube formation of endothelial cells [65,66] and therefore may possibly influence HUVECs behaviour as well.

Despite the primary role of monoculture systems in the early stages of research, those models suffer substantial limitations as they lack any interactions among cells of different origins. Therefore, inclusion of multiple cell types must be considered when attempting to approximate the *in vivo* situation.

The complementary relationships of MSCs, osteoblasts, fibroblasts, and immune cells with endothelial cells, which are certainly vital for proper fracture repair, are an exemplary case [30,47,67,68]. In the initial stages of bone healing, immune cells guide the inflammatory response and the onset of angiogenesis. A description of the relationship between macrophages and ECs showed an improved angiogenic response of ECs attained in conditioned medium from stimulated mouse monocytes [47]. The interactions of MSCs/osteoblastic cells with ECs, commonly used for coculture models of bone fracture-related angiogenesis and also investigated in this study, develop later in the healing process. Endothelial cells thrive in the presence of MSCs/osteoblasts and vice versa. The angiogenic and osteogenic differentiation potentials are higher in comparison to respective monocultures, leading to successful bone regeneration [69,70]. MSCs belong to a group of cell types capable of VEGF secretion, which can mediate the endothelial differentiation, proliferation, and migration via paracrine signalling pathways [21,71,72]. Studies have shown that cocultures of ECs and MSCs were beneficial for differentiation of endothelial phenotype and expression of specific markers, such as CD31 and von Willebrand factor, likely due to the delivery of VEGF to endothelial cells [71]. The symbiotic relationship of the coculture has also been illustrated by the mutual attachment of MSCs and ECs (particularly endothelial progenitor cells), which augmented the pluripotency of MSCs and simultaneously promoted angiogenesis [73].

Under optimal conditions, production of angiogenic cytokines by MSCs/osteoblastic cells can be increased. The use of strontium-containing biomaterials was reported to stimulate MSCs/osteoblastic cells towards higher secretion of VEGF [23,29,74,75] and platelet-derived growth factor (PDGF)-BB [21], which are both essential for angiogenesis. The subsequent use of such conditioned media with supplementary growth factors for culturing of ECs ensured greater NO production [76] and augmented recruitment and tube formation capacity of HUVECs [21,77]. A direct coculture of HUVECs and osteoblastic cells on strontium containing scaffolds (SCPP) promoted growth, proliferation of both cell types and increased expression of endothelial markers (PECAM1) and resulted in generation of longer tubular structures, implying its angiogenic character for *in vivo* application [30,62].

In this study, conditioned media obtained from MSCs cultured with and without strontium were used for cultivation of HUVECs seeded on PT and PT-Sr implants. Experimental groups containing either of the two conditioned media exhibited elevated VEGF and FGF-21 concentration, in comparison to the EGM group (HUVECs cultured in unmodified EGM-2 medium), implying that the coculture systems possessed greater angiogenic potential in comparison to the monoculture of ECs. However, the detected protein concentration was a cumulative contribution from both cell types, necessitating additional experiments to determine the augmenting effects of the CM on the VEGF and FGF-21 secretion by HUVECs seeded on PT and PT-Sr implants.

As addressed earlier in this section, host response to a material is not a single-cell operation, but rather a result of complex signalling pathways mediating communication among various cell types, which modulate the quality of the developing cell-material interface. For instance, an inconsistent response of HUVECs to titanium substrates was observed, when culturing those cells alone or together with osteoblastic cells. Researchers found, that monocultured HUVECs preferred smooth hydrophilic surfaces, while in coculture they exhibited higher viability and proliferation rates on smooth hydrophobic material [63]. This finding clearly evinced some of the inaccuracies manifested by monoculture systems and provided substantial evidence that cellular responses are controlled not only by the surface characteristics but guided also by presence and maturation/differentiation of other cell types.

5 Conclusions

The aim of this study was to investigate the effects of strontium releasing titanium implants on the behaviour of HUVECs. Therefore, 3D printed implants were surface modified by plasma electrolytic oxidation (PEO) in electrolytes with/without Sr additions. Surfaces with comparable topography and distinct chemical composition were successfully produced by optimization of the PEO conditions. The in vitro tests conducted in this study with HUVECs did not reveal any enhancing effects of either of the tested surfaces on the morphology, proliferation, wound healing and differentiation of HUVECs. The implants topography and associated microroughness presented on the surfaces appeared to be rather suboptimal for long-term attachment, proliferation and migration of endothelial cells, which can be explained by their preference for physiologically more natural smooth surfaces. It should be noted that those implants were designed primarily for bone cells and intended to promote their osteogenic differentiation and deposition of new bone tissue. Therefore, before performing any optimization of this implant design, further experiments need to be conducted to assess the response of HUVECs to those surfaces in a more complex environment (coculture) and to validate the actual cause for the observed endothelial behaviour. Only then, a proper conclusion about the implants ability to promote early deposition of well-vascularized bone, which would secure a stronger connection with the implant, can be made.

6 Reflection on limitations and future recommendations

This work was a continuation to a past study investigating the effects of the strontium incorporating implants on preosteoblastic cells [39]. The implants utilized in this study had been optimized for bone cells and possessed optimal osteogenic surface properties. They were presented with macroporosity by design, microroughness by manufacturing method and submicron porosity and distinct chemical composition by PEO treatment, with the later three being known cues guiding cellular response.

The use of a new cell type necessitated adjustments to experimental protocols adopted from previous work with MSCs/preosteoblasts (MC3T3-E1), by optimising individual steps with consideration to the properties of HUVECs. A major challenge encountered during this project was the unexpected behaviour of HUVECs on the implants' surfaces throughout the performed assays. The seeding efficiency of HUVECs was satisfactory and comparable with that of MSCs/preosteoblasts. Throughout the monitoring period, however, HUVECs were found to gradually fall off/leave the implant's surface. This behaviour posed a fundamental hindrance for some assays; low and varying number of cells obtained from the implants yielded unreliable data with large variability when performing absolute count of cells detached from the implants. It also introduced obstacles for analysis of gene expression due to low number of available replicates with sufficient amount of extracted cellular material (RNA).

The possible effects of the combination of the physical and chemical cues presented on the surfaces on HUVECs were elaborated in the previous section (discussion). Findings from past research indicated that the residual metal particles on the implants could hinder clustering of HUVECs and thereby impede further proliferation and migration of those cells. To validate this assumption, further tests need to be performed. It would be advisable to decouple the variables possibly affecting the cellular response and test them individually in separate experimental setups. The effect of chemical composition can be tested in extracts obtained from the implants. The role of microroughness can be further evaluated by assessing response of HUVECs to (flat) casted PEO treated implants, which do not bear the round particles on their surfaces.

The assessment can be carried out by checking the variability in expression levels of angiogenic (e.g. VEGF, HIF1- α, PECAM1, FGF-21) and attachment markers (e.g. α5β1, αvβ3, αvβ5) after exposing cells to the different extracts and surfaces. Furthermore, proliferation and wound healing can be assessed, as performed in this study to reach understanding about the ongoing intracellular processes driving the observable interaction with other cell types and extracellular responses to the material.

However, care should be taken while implementing those results in the future designs. It should be acknowledged that those implants were primarily intended for MSCs/osteoblastic cells which prosper on the micro- and nanorough surfaces, while the macroporosity ensures a more stable fixation of the implants in the regenerated bone tissue. Moreover, the selected strontium concentration was also proven to guide the osteogenic differentiation of bone cells and augment the bone matrix deposition. Changing those parameters to exclusively benefit ECs may compromise the osteogenic properties of the implants which, however, should remain the primary focus.

The experiments conducted thus far implied slightly suboptimal character of the surfaces for HUVECs but at the same time did not reveal any alarming inhibitory effects. Only further tests examining also functional properties of HUVECs (such as sprouting) in 3D environment and their behaviour in more

complex coculture systems, reflecting more closely the clinical situation, will determine the necessity for any changes and the actual potential of these implants to enhance osseointegration.

7 Bibliography

[1] Karachalios, T.; Komnos, G.; Koutalos, A. Total Hip Arthroplasty: Survival and Modes of Failure. *EFORT Open Rev.*, **2018**, *3*, 232–239.

[2] Raphel, J.; Holodniy, M.; Goodman, S.B.; Heilshorn, S.C. Multifunctional Coatings to Simultaneously Promote Osseointegration and Prevent Infection of Orthopaedic Implants. *Biomaterials*, **2016**, *84*, 301–314.

[3] Delaunay, C.; Hamadouche, M. What Are the Causes for Failures of Primary Hip Arthroplasties in France ? **2013**, 3863–3869.

[4] Parithimarkalaignan, S.; Padmanabhan, T. V. Osseointegration: An Update. *J. Indian Prosthodont. Soc.*, **2013**, *13*, 2–6.

[5] Yu, X.; Tang, X.; Gohil, S. V; Laurencin, C.T. Biomaterials for Bone Regenerative Engineering. *Adv. Healthc. Mater.*, **2015**, *4*, 1268–1285.

[6] Awad, N.K.; Edwards, S.L.; Morsi, Y.S. A Review of TiO2 NTs on Ti Metal: Electrochemical Synthesis, Functionalization and Potential Use as Bone Implants. *Mater. Sci. Eng. C*, **2017**, *76*, 1401–1412.

[7] Sumner, D.R. Long-Term Implant Fixation and Stress-Shielding in Total Hip Replacement. *J. Biomech.*, **2015**, *48*, 797–800.

[8] Kulkarni, M.; Mazare, A.; Schmuki, P.; Iglič, A. Biomaterial Surface Modification of Titanium and Titanium Alloys for Medical Applications. *Nanomedicine*, 111–136.

[9] Jones, L.C.; Timmie Topoleski, L.D.; Tsao, A.K. *Biomaterials in Orthopaedic Implants*; Elsevier Ltd., **2017**.

[10] Code, R.; Type, L. *Orthopedic Biomaterials 2009*; **2009**.

[11] Sidhu, S.S. *Biomaterials in Orthopaedics and Bone Regeneration*; **2019**.

[12] Lin, S.H.; Zhang, W.J.; Jiang, X.Q. Applications of Bioactive Ions in Bone Regeneration. *Chinese J. Dent. Res.*, **2019**, 93–104.

[13] Hoppe, A.; Güldal, N.S.; Boccaccini, A.R. A Review of the Biological Response to Ionic Dissolution Products from Bioactive Glasses and Glass-Ceramics. *Biomaterials*, **2011**, *32*, 2757–2774.

[14] Marsell, R.; Einhorn, T.A. The Biology of Fracture Healing. *Injury*, **2011**, *42*, 551–555.

[15] Kolte, D.; Mcclung, J.A.; Aronow, W.S. Chapter 6. Vasculogenesis and Angiogenesis. In: *Translational Research in Coronary Artery Disease*; Elsevier Inc., **2016**; pp. 49–66.

[16] Shrivats, A.R.; Alvarez, P.; Schutte, L.; Hollinger, J.O. Bone Regeneration. In: *Principles of Tissue Engineering*; Elsevier, **2014**; pp. 1201–1221.

[17] Bahney, C.S.; Zondervan, R.L.; et al. Cellular Biology of Fracture Healing. *J. Orthop. Res.*, **2019**, *37*, 35–50.

[18] Kolar, P.; Gaber, T.; Perka, C. Human Early Fracture Hematoma Is Characterized by Inflammation and Hypoxia. *Clin. Orthop. Relat. Res.*, **2011**, *469*, 3118–3126.

[19] Hankenson, K.D.; Dishowitz, M.; Gray, C.; Schenker, M. Angiogenesis in Bone Regeneration. *Injury*, **2012**, *42*, 556–561.

[20] Stegen, S.; Gastel, N. Van; Carmeliet, G. Bringing New Life to Damaged Bone: The Importance of Angiogenesis in Bone Repair and Regeneration. *Bone*, **2015**, *70*, 19–27.

[21] Zhang, W.; Cao, H.; Zhang, X.; Li, G.; Chang, Q.; Zhao, J.; Qiao, Y.; Ding, X.; Yang, G.; Liu, X.; Jiang, X. A Strontium-Incorporated Nanoporous Titanium Implant Surface for Rapid Osseointegration. *Nanoscale*, **2016**, 5291–5301.

[22] Lakhkar, N.J.; Lee, I.; Kim, H.; Salih, V.; Wall, I.B.; Knowles, J.C. Bone Formation Controlled by Biologically Relevant Inorganic Ions: Role and Controlled Delivery from Phosphate-Based Glasses. *Adv. Drug Deliv. Rev.*, **2013**, *65*, 405–420.

[23] Guo, X.; Wei, S.; Lu, M.; Shao, Z.; Lu, J.; Xia, L.; Lin, K. Dose-Dependent Effects of Strontium Ranelate on Ovariectomy Rat Bone Marrow Mesenchymal Stem Cells and Human Umbilical Vein Endothelial Cells. *Int. J. Biol. Sci.*, **2016**, *12*, 1511–1522.

[24] Wang, G.; Zhang, W.; Lv, K. Effects of Sr-HT-Gahnite on Osteogenesis and Angiogenesis by Adipose Derived Stem Cells for Critical-Sized Calvarial Defect Repair. *Sci. Rep.*, **2017**, *7*, 41135–41145.

[25] Chen, Y.W.; Shi, G.Q.; Ding, Y.L.; Yu, X.X.; Zhang, X.H.; Zhao, C.S.; Wan, C.X. In Vitro Study on the Influence of Strontium-Doped Calcium Polyphosphate on the Angiogenesis-Related Behaviors of HUVECs. *J. Mater. Sci. Mater. Med.*, **2008**, *19*, 2655–2662.

[26] Chen, Y.W.; Feng, T.; Shi, G.Q.; Ding, Y.L.; Yu, X.X.; Zhang, X.H.; Zhang, Z.B.; Wan, C.X. Interaction of Endothelial Cells with Biodegradable Strontium-Doped Calcium Polyphosphate for Bone Tissue Engineering. *Appl. Surf. Sci.*, **2008**, *255*, 331–335.

[27] Jebahi, S.; Oudadesse, H.; Feki, H.; Rebai, T.; Keskes, H.; Pellen, P. Antioxidative / Oxidative Effects of Strontium-Doped Bioactive Glass as Bone Graft . In Vivo Assays in Ovariectomised Rats. *J. Appl. Biomed.*, **2012**, *10*, 195–209.

[28] Lin, K.; Xia, L.; Li, H.; Jiang, X.; Pan, H.; Xu, Y.; Lu, W.W.; Zhang, Z.; Chang, J. Enhanced Osteoporotic Bone Regeneration by Strontium-Substituted Calcium Silicate Bioactive Ceramics. *Biomaterials*, **2013**, *34*, 10028–10042.

[29] Wang, X.; Wang, Y.; Li, L.; Gu, Z.; Xie, H.; Yu, X. Stimulations of Strontium-Doped Calcium Polyphosphate for Bone Tissue Engineering to Protein Secretion and MRNA Expression of the Angiogenic Growth Factors from Endothelial Cells in Vitro. *Ceram. Int.*, **2014**, *40*, 6999–7005.

[30] Gu, Z.; Xie, H.; Huang, C.; Peng, H.; Tan, H. Effects of Strontium-Doped Calcium Polyphosphate on Angiogenic Growth Factors Expression of Co-Culturing System in Vitro and of Host Cell in Vivo. *RSC Adv.*, **2014**, *4*, 2783–2792.

[31] Bellucci, D.; Braccini, S.; Chiellini, F.; Balasubramanian, P.; Boccaccini, A.R.; Cannillo, V. Bioactive Glasses and Glass-Ceramics versus Hydroxyapatite : Comparison of Angiogenic Potential and Biological Responsiveness. **2019**, 2601–2609.

[32] Andrea, L.D.D.; Romanelli, A.; Stasi, D.; Pedone, C.; Andrea, L.D. Bioinorganic Aspects of Angiogenesis. **2010**, 7625–7636.

[33] Echeverry-Rendón, M.; Galvis, O.; Giraldo, D.Q.; López-lacomba, J.L. Osseointegration Improvement by Plasma Electrolytic Oxidation of Modified Titanium Alloys Surfaces. *J.*

Mater. Sci. Mater. Med., **2015**, *26*, 1–18.

[34] Hartjen, P.; Hoffmann, A.; Henningsen, A.; Barbeck, M.; Kopp, A.; Kluwe, L.A.N.; Precht, C.; Quatela, O.; Gaudin, R.; Heiland, M.A.X.; Friedrich, R.E.; Knipfer, C.; Grubeanu, D.; Smeets, R.; Jung, O.L.E. Plasma Electrolytic Oxidation of Titanium Implant Surfaces : Microgroove-Structures Improve. *Int. J. Exp. Clin. Pathophysiol. Drug Res.*, **2018**, *247*, 241–247.

[35] Guan, Y. Nanotubular Surface Modification of Metallic Implants via Electrochemical Anodization Technique. *Int. J. Nanomedicine*, **2014**, *9*, 4421–4435.

[36] Kulkarni, M. Titanium Nanostructures for Biomedical Applications. *Nanotechnology*, **2015**, *26*, 1–18.

[37] Santos-Coquillat, A.; Esteban-Lucia, M.; Martinez-Campos, E.; Mohedano, M.; Arrabal, R. PEO Coatings Design for Mg-Ca Alloy for Cardiovascular Stent and Bone Regeneration Applications. *Mater. Sci. Eng. C*, **2019**, *105*, 110026–110044.

[38] Teng, H.P.; Lin, H.Y.; Huang, Y.H.; Lu, F.H. Formation of Strontium-Substituted Hydroxyapatite Coatings on Bulk Ti and TiN-Coated Substrates by Plasma Electrolytic Oxidation. *Surf. Coatings Technol.*, **2018**, *350*, 1112–1119.

[39] van Hengel, I.A.J.; Gelderman, F.S.A.; Athanasiadis, S.; Minneboo, M.; Weinans, H.; Fluit, A.C.; van der Eerden, B.C.J.; Fratila-Apachitei, L.E.; Apachitei, I.; Zadpoor, A.A. Functionality-Packed Additively Manufactured Porous Titanium Implants. *Mater. Today Bio*, **2020**, *7*, 100060–100071.

[40] van Hengel, I.A.J.; Riool, M.; Fratila-Apachitei, L.E.; Witte-Bouma, J.; Farrell, E.; Zadpoor, A.A.; Zaat, S.A.J.; Apachitei, I. Selective Laser Melting Porous Metallic Implants with Immobilized Silver Nanoparticles Kill and Prevent Biofilm Formation by Methicillin-Resistant Staphylococcus Aureus. *Biomaterials*, **2017**, *140*, 1–15.

[41] Bruedigam, C.; van Driel, M.; Koedam, M.; van de Peppel, J.; van der Eerden, B.C.J.; Eijken, M.; van Leeuwen, J.P.T.M. Basic Techniques in Human Mesenchymal Stem Cell Cultures: Differentiation into Osteogenic and Adipogenic Lineages, Genetic Perturbations, and Phenotypic Analyses. *Curr. Protoc. Stem Cell Biol.*, **2011**, 1–20.

[42] Shin, K.R.; Ko, Y.G.; Shin, D.H. Effect of Electrolyte on Surface Properties of Pure Titanium Coated by Plasma Electrolytic Oxidation. *J. Alloys Compd.*, **2011**, *509*, S478–S481.

[43] Durdu, S.; Deniz, Ö.F.; Kutbay, I.; Usta, M. Characterization and Formation of Hydroxyapatite on Ti6Al4V Coated by Plasma Electrolytic Oxidation. *J. Alloys Compd.*, **2013**, *551*, 422–429.

[44] Fazel, M.; Salimijazi, H.R.; Shamanian, M.; Minneboo, M.; Modaresifar, K.; Hengel, I.A.J. Van; Fratila-apachitei, L.E.; Apachitei, I.; Zadpoor, A.A. Osteogenic and Antibacterial Surfaces on Additively Manufactured Porous Ti-6Al-4V Implants : Combining Silver Nanoparticles with Hydrothermally Synthesized HA Nanocrystals. *Mater. Sci. Eng. C*, **2020**, *120*, 111745–111758.

[45] Saidak, Z.; Marie, P.J. Strontium Signaling : Molecular Mechanisms and Therapeutic Implications in Osteoporosis. *Pharmacol. Ther.*, **2012**, *136*, 216–226.

[46] Stepan, J.J. Strontium Ranelate : In Search for the Mechanism of Action. *J. Bone Miner. Metab.*, **2013**, *31*, 606–612.

[47] Zhao, F.; Lei, B.; Li, X.; Mo, Y.; Wang, R. Promoting in Vivo Early Angiogenesis with Sub-

Micrometer Strontium- Contained Bioactive Microspheres through Modulating Macrophage Phenotypes. *Biomaterials*, **2018**, *178*, 36–47.

[48] Mohan, C.C.; Sreerekha, P.R.; Divyarani, V. V; Nair, S.; Chennazhi, K. Influence of Titania Nanotopography on Human Vascular Cell Functionality and Its Proliferation in Vitro †. *J. Mater. Chem.*, **2012**, *22*, 1326–1340.

[49] Tan, A.W.; Liau, L.L.; Chua, K.H.; Ahmad, R.; Akbar, S.A.; Pingguan-Murphy, B. Enhanced in Vitro Angiogenic Behaviour of Human Umbilical Vein Endothelial Cells on Thermally Oxidized TiO 2 Nanofibrous Surfaces. *Sci. Rep.*, **2016**, *6*, 1–10.

[50] Lu, J.; Khang, D.; Webster, T.J. Greater Endothelial Cell Responses on Submicron and Nanometer Rough Titanium Surfaces. *J. Biomed. Mater. Res. - Part A*, **2010**, *94*, 1042–1049.

[51] Gentile, F.; Tirinato, L.; Battista, E.; Causa, F.; Liberale, C.; di Fabrizio, E.M.; Decuzzi, P. Cells Preferentially Grow on Rough Substrates. *Biomaterials*, **2010**, *31*, 7205–7212.

[52] Gong, Z.; Cheng, H.; Zhang, M.; Liu, X.; Zeng, Y.; Xiang, K.; Xu, Y.; Wang, Y.; Zhu, Z. Osteogenic Activity and Angiogenesis of a SrTiO3 Nano-Gridding Structure on Titanium Surface. *J. Mater. Chem. B*, **2017**, *5*, 537–552.

[53] Lin, Y.; Shao, Y.; Li, J.; Zhang, W.; Zheng, K.; Zheng, X.; Huang, X.; Liao, Z.; Xie, Y.; He, J. The Hierarchical Micro-/Nanotextured Topographies Promote the Proliferation and Angiogenesis-Related Genes Expression in Human Umbilical Vein Endothelial Cells by Initiation of Hedgehog-Gli1 Signaling. *Artif. Cells, Nanomedicine Biotechnol.*, **2018**, *46*, S1141–S1151.

[54] Huang, L.; Cui, L.; Kim, D.H.; Joo, H.J.; Seo, H.; Choi, S.; Noh, J.; Lee, K.B.; Hong, S.J. Regulating Response and Leukocyte Adhesion of Human Endothelial Cell by Gradient Nanohole Substrate. *Sci. Rep.*, **2019**, *9*, 1–11.

[55] Rodrigues, T.; Gomes, M.E.; Leite, A.J.; Gonc, A.I.; Mano, F. Strontium-Doped Bioactive Glass Nanoparticles in Osteogenic Commitment. *Appl. Mater. Interfaces*, **2018**, *10*, 23311–23320.

[56] Lai, M.; Yang, X.; Liu, Q.; Li, J.; Hou, Y.; Chen, X. The Surface Nanostructures of Titanium Alloy Regulate the Proliferation of Endothelial Cells. *AIMS Mater. Sci.*, **2014**, *1*, 45–58.

[57] Ren, X.; Feng, Y.; Guo, J.; Wang, H.; Li, Q.; Yang, J.; Hao, X.; Lv, J.; Ma, N.; Li, W. Surface Modification and Endothelialization of Biomaterials as Potential Scaffolds for Vascular Tissue Engineering Applications. *Chem. Soc. Rev.*, **2015**, *44*, 5680–5742.

[58] Post, A.; Wang, E.; Cosgriff-Hernandez, E. A Review of Integrin-Mediated Endothelial Cell Phenotype in the Design of Cardiovascular Devices. *Ann. Biomed. Eng.*, **2019**, *47*, 366–380.

[59] Skrzypek, K.; Nibbelink, M.G.; Karbaat, L.P.; Karperien, M.; van Apeldoorn, A.; Stamatialis, D. An Important Step towards a Prevascularized Islet Macroencapsulation Device—Effect of Micropatterned Membranes on Development of Endothelial Cell Network. *J. Mater. Sci. Mater. Med.*, **2018**, *29*.

[60] Wang, W.Y.; Lin, D.; Jarman, E.H.; Polacheck, W.J.; Baker, B.M. Functional Angiogenesis Requires Microenvironmental Cues Balancing Endothelial Cell Migration and Proliferation. *Lab Chip*, **2020**, *20*, 1153–1166.

[61] An, N.; Schedle, A.; Wieland, M.; Andrukhov, O.; Matejka, M.; Rausch-Fan, X. Proliferation,

Behavior, and Cytokine Gene Expression of Human Umbilical Vascular Endothelial Cells in Response to Different Titanium Surfaces. *J. Biomed. Mater. Res. - Part A*, **2010**, *93*, 364–372.

[62] Gu, Z.; Xie, H.; Li, L.; Zhang, X. Application of Strontium-Doped Calcium Polyphosphate Scaffold on Angiogenesis for Bone Tissue Engineering. *J. Mater. Sci. Mater. Med.*, **2013**, *24*, 1251–1260.

[63] Shi, B.; Andrukhov, O.; Berner, S.; Schedle, A.; Rausch-Fan, X. The Angiogenic Behaviors of Human Umbilical Vein Endothelial Cells (HUVEC) in Co-Culture with Osteoblast-like Cells (MG-63) on Different Titanium Surfaces. *Dent. Mater.*, **2014**, *30*, 839–847.

[64] Zhu, H.; Zhai, D.; Lin, C.; Zhang, Y.; Huan, Z.; Chang, J.; Wu, C. 3D Plotting of Highly Uniform Sr5(PO4)2SiO4 Bioceramic Scaffolds for Bone Tissue Engineering. *J. Mater. Chem. B*, **2016**, 6200–6212.

[65] Munaron, L. Intracellular Calcium, Endothelial Cells and Angiogenesis. *Recent Pat. Anticancer. Drug Discov.*, **2006**, *1*, 105–119.

[66] Moccia, F.; Negri, S.; Shekha, M.; Faris, P.; Guerra, G. Endothelial Ca2+ Signaling, Angiogenesis and Vasculogenesis: Just What It Takes to Make a Blood Vessel. *Int. J. Mol. Sci.*, **2019**, *20*, 1–39.

[67] Fu, W.-L.; Xiang, Z.; Huang, F.-G. Coculture of Peripheral Blood-Derived Mesenchymal Stem Cells and Endothelial Progenitor Cells on Strontium-Doped Calcium Polyphosphate Scaffolds to Generate Vascularized Engineered Bone. *Tissue Eng. Part A*, **2015**, *21*, 948–959.

[68] Choong, C.S.N.; Hutmacher, D.W.; Triffitt, J.T. Co-Culture of Bone Marrow Fibroblasts and Endothelial Cells on Modified Polycaprolactone Substrates for Enhanced Potentials in Bone Tissue Engineering. *Tissue Eng.*, **2006**, *12*.

[69] Simunovic, F.; Winninger, O.; Strassburg, S.; Koch, H.G.; Finkenzeller, G.; Stark, G.B.; Lampert, F.M. Increased Differentiation and Production of Extracellular Matrix Components of Primary Human Osteoblasts after Cocultivation with Endothelial Cells: A Quantitative Proteomics Approach. *J. Cell. Biochem.*, **2019**, 396–404.

[70] Paul, D.; Herzog, E.; Dohle, E.; Bischoff, I.; Kirkpatrick, C.J. Cell Communication in a Coculture System Consisting of Outgrowth Endothelial Cells and Primary Osteoblasts. *Biomed. Res. Int.*, **2014**, *2014*, 1–15.

[71] Ge, Q.; Zhang, H.; Hou, J.; Wan, L.; Cheng, W.; Wang, X.; Dong, D.A.N.; Chen, C.; Xia, J.I.E.; Guo, J.U.N.; Chen, X.; Wu, X. VEGF Secreted by Mesenchymal Stem Cells Mediates the Differentiation of Endothelial Progenitor Cells into Endothelial Cells via Paracrine Mechanisms. *Mol. Med. Rep.*, **2018**, *17*, 1667–1675.

[72] Yang, X.; Jiang, J.; Zhou, L.; Wang, S.; He, M.; Luo, K.; Chen, Y.; Xu, X. Osteogenic and Angiogenic Characterization of Mandible and Femur Osteoblasts. *J. Mol. Histol.*, **2019**, *50*, 105–117.

[73] Xia, J.; Zhang, H.; Gao, X.; Guo, J.; Hou, J.; Wang, X.; Wang, S.; Yang, T.; Zhang, X.; Ge, Q.; Wan, L.; Cheng, W.; Zheng, J. E-Cadherin-Mediated Contact of Endothelial Progenitor Cells with Mesenchymal Stem Cells through b -Catenin Signaling. **2016**, *40*, 407–418.

[74] Liu, F.; Zhang, X.; Yu, X.; Xu, Y. In Vitro Study in Stimulating the Secretion of Angiogenic

Growth Factors of Strontium-Doped Calcium Polyphosphate for Bone Tissue Engineering. *J. Mater. Sci. Mater. Med.*, **2011**, 683–692.

[75] Strobel, L.A.; Hild, N.; Mohn, D.; Stark, W.J.; Hoppe, A.; Gbureck, U.; Horch, R.E.; Kneser, U.; Boccaccini, A.R. Novel Strontium-Doped Bioactive Glass Nanoparticles Enhance Proliferation and Osteogenic Differentiation of Human Bone Marrow Stromal Cells. **2013**.

[76] Chen, Y.; Gao, A.; Bai, L.; Wang, Y.; Wang, X.; Zhang, X.; Huang, X.; Hang, R.; Tang, B.; Chu, P.K. Antibacterial, Osteogenic, and Angiogenic Activities of SrTiO3 Nanotubes Embedded with Ag2O Nanoparticles. *Mater. Sci. Eng. C*, **2017**, *75*, 1049–1058.

[77] Chen, Y.; Zheng, Z.; Zhou, R.; Zhang, H.; Chen, C.; Xiong, Z.; Liu, K.; Wang, X. Developing a Strontium-Releasing Graphene Oxide- / Collagen-Based Organic − Inorganic Nanobiocomposite for Large Bone Defect Regeneration via MAPK Signaling Pathway. *ACS Appl. Mater. Interfaces*, **2019**, *11*, 15986–15997.

[78] Li, J.; Kacena, M.A.; Stocum, D.L. *Fracture Healing*; Second Edi.; Elsevier Inc., **2019**.

[79] Einhorn, T.A.; Gerstenfeld, L.C.; Surgery, O.; Avenue, H.; Surgery, O. Fracture Healing : Mechanisms and Interventions. *Nat. Rev. Rheumatol.*, **2015**, *11*, 45–54.

[80] Loi, F.; Cordova, L.A.; Pajarinen, J.; Lin, T.; Yao, Z.; Goodman, S.B. Inflammation, Fracture and Bone Repair. *Bone*, **2016**, *86*, 119–130.

[81] Bahney, C.S.; Zondervan, R.L.; Allison, P.; Theologis, A.; Ashley, J.W.; Ahn, J.; Miclau, T.; Marcucio, R.S.; Hankenson, K.D. Cellular Biology of Fracture Healing. *J. Orthop. Res.*, **2019**, *37*, 35–50.

[82] Claes, L.; Recknagel, S.; Ignatius, A. Fracture Healing under Healthy and Inflammatory Conditions. *Nat. Rev. Rheumatol.*, **2012**, *8*, 133–143.

[83] Oryan, A.; Monazzah, S.; Bigham-sadegh, A. Bone Injury and Fracture Healing Biology. *Biomed. Environ. Sci.*, **2015**, *28*, 57–71.

[84] Sivaraj, K.K.; Adams, R.H. Blood Vessel Formation and Function in Bone. *Development*, **2016**, 2706–2715.

[85] Maes, C.; Kobayashi, T.; Selig, M.K.; Torrekens, S.; Roth, S.I.; Mackem, S.; Carmeliet, G.; Kronenberg, H.M. Osteoblast Precursors, but Not Mature Osteoblasts, Move into Developing and Fractured Bones along with Invading Blood Vessels. *Dev. Cell*, **2010**, *19*, 329–344.

[86] Maes, C.; Clemens, T.L. Angiogenic–Osteogenic Coupling: The Endothelial Perspective. *Bonekey Rep.*, **2014**, *3*, 1–4.

[87] Ackermann, M.; Houdek, J.P.; Gibney, B.C.; Ysasi, A. Sprouting and Intussusceptive Angiogenesis in Postpneumonectomy Lung Growth : Mechanisms of Alveolar Neovascularization. *Angiogenesis*, **2014**, 541–551.

[88] Djukic, T.; Kim, J.; Zuber, B.; Makanya, A. Synergistic Interaction of Sprouting and Intussusceptive Angiogenesis during Zebrafish Caudal Vein Plexus Development. *Sci. Rep.*, **2018**, *8*, 1–15.

[89] Potente, M.; Gerhardt, H.; Carmeliet, P. Basic and Therapeutic Aspects of Angiogenesis. *Cell*, **2011**, *146*, 873–887.

[90] Milkiewicz, M.; Ispanovic, E.; Doyle, J.L.; Haas, T.L. Regulators of Angiogenesis and Strategies

for Their Therapeutic Manipulation. *Int. J. Biochem. Cell Biol.*, **2006**, *38*, 333–357.

[91] Lertkiatmongkol, P.; Liao, D.; Mei, H.; Hu, Y.; Peter, J.; Hospital, U. Endothelial Functions of PECAM-1 (CD31). *Curr. Opin. Hematol.*, **2017**, *23*, 253–259.

[92] Li, Y.; Huang, J.; Jiang, Z.; Jiao, Y.; Wang, H. FGF21 Inhibitor Suppresses the Proliferation and Migration of Human Umbilical Vein Endothelial Cells through the ENOS/PI3K/AKT Pathway. *Am. J. Transl. Res.*, **2017**, *9*, 5299–5307.

[93] Huang, W.; Shao, M.; Liu, H.; Chen, J.; Hu, J.; Zhu, L.; Liu, F.; Wang, D.; Zou, Y.; Xiong, Y.; Wang, X. Fibroblast Growth Factor 21 Enhances Angiogenesis and Wound Healing of Human Brain Microvascular Endothelial Cells by Activating PPARγ. *J. Pharmacol. Sci.*, **2019**, *140*, 120–127.

[94] Yaqoob, U.; Jagavelu, K.; Shergill, U.; De Assuncao, T.; Cao, S.; Shah, V.H. FGF21 Promotes Endothelial Cell Angiogenesis through a Dynamin-2 and Rab5 Dependent Pathway. *PLoS One*, **2014**, *9*.

8 Appendix

8.1 Abbreviations

αMEM	Minimum essential medium α
ANG-1/2	Angiopoietin 1/2
BED	Backscattered electron detector
(B)MSCs	(Bone marrow-derived) mesenchymal stem cells
BSA	Bovine serum albumin
CaSR	Calcium sensing receptor
cc	Coculture
CD31	Cluster of differentiation 31
CM	Conditioned medium
d	Days
DAPI	4′,6-diamidino-2-phenylindole
ECs	Endothelial cells
EDS	Energy-dispersive X-ray spectroscopy
EdU	5-ethynyl-2’-deoxyuridine
EGM-2	Endothelial cell growth medium 2
ELISA	Enzyme-linked immunosorbent assay
EPCs	Endothelial progenitor cells
FCS	Fetal calf serum
FGF	Fibroblast growth factor
h	Hours
HA	Hydroxyapatite
hADSC	Human adipose-derived stem cells
HEPES	4-(2-hydroxyethyl)-1-piperazineethanesulfonic acid)
HIF1-α	Hypoxia inducible factor 1 alpha
HUVECs	Human umbilical vein endothelial cells
IRP	Ion release profile
MAO	Microarc oxidation
MC	Material composition
MMPs	Matrix metallopeptidases/ metalloproteinases
NO	Nitric oxide
OB	Osteoblasts/osteoblastic cells
OD	Optical density
PBS	Phosphate-buffered saline
PDGFs	Platelet-derived growth factor
PECAM1	Platelet endothelial cell adhesion molecule
PEO	Plasma electrolytic oxidation
PT(-Sr)	PEO treated sample (with strontium)
rhEGF	Recombinant human epidermal growth factor

rhFGF	Recombinant human fibroblast growth factor
RT-qPCR	Reverse transcription-quantitative polymerase chain reaction
s	Seconds
(S)CPP	(Strontium) calcium polyphosphate
SED	Secondary electron detector
SEM	Scanning electron microscopy
SrA	Strontium acetate
TCP	Tricalcium phosphate
TGF-β	Transforming growth factor beta
THA	Total hip arthroplasty
TJR	Total joint replacement
VEGF	Vascular endothelial growth factor
w	weeks

8.2 List of figures and tables

8.3 Supplementary material

8.3.1 Angiogenesis and its role in fracture healing

After a bone replacement surgery, the body suffers local tissue damage analogous to that of a fracture. The blood supply is disrupted and the local environment loses mechanical stability [16,78]. New bone and vascular tissue must both be generated to restore homeostasis. The mutual dependence of angiogenesis and osteogenesis has been recognized by many studies as being critical for achieving successful bone repair, as impaired angiogenic ability or significantly damaged vasculature has been associated with increased occurrence of nonunions or delayed repair [18,19,79–81]. The fracture healing process is illustrated in Figure 14.

In the immediate aftermath of tissue damage, the wound elicits inflammatory and haemostatic reactions, defined by orchestrated molecular cascades, blood vessel constriction, blood coagulation, and the formation of a fibrin-rich blood clot at the affected site [18,80,82]. The clot is characterized by hypoxia and low pH and serves as a temporary scaffold at the wounded site [18]. It is also a source for cytokines and signalling molecules, which together with environmental factors (hypoxia) are responsible for the recruitment of MSCs, endothelial progenitor cells (EPCs), and inflammatory cells from their local sources [14,17,78,82,83].

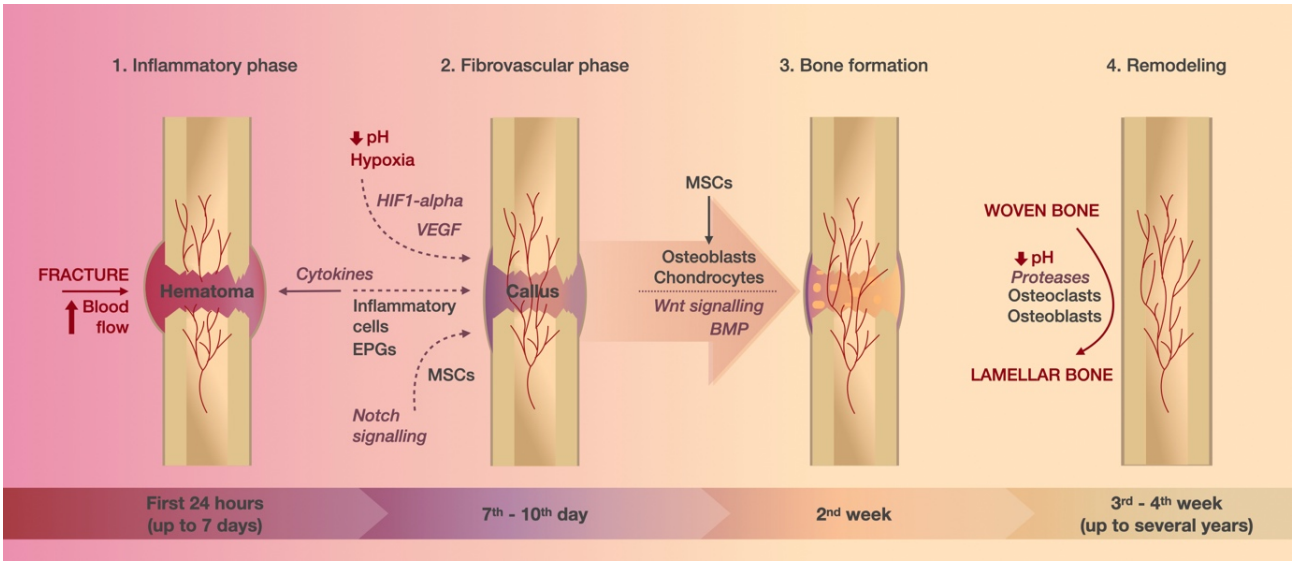

Figure 14. An illustration depicting the stages of fracture healing: 1) In the initial inflammatory phase (lasting up to 7 days after injury), the increased blood delivery to the affected site results in the formation of hematoma with a high content of cytokines; 2) Cells attracted by cytokines and environmental factors (hypoxia, low pH, HIF1-alpha, VEGF) are responsible for the repair of damaged vessels and formation of provisional fibrous tissue called callus (7-10 days after injury); 3) At around two weeks after injury, MSCs undergo differentiation into osteoblasts and chondrocytes governed by Wnt and BMP signalling and provisional woven bone is generated; 4) In the final phase starting 3-4 weeks after injury and lasting up to several years, the woven bone is replaced by lamellar bone.

The initial inflammatory reaction has a substantial influence on the formation of a callus, *i.e.* a fibrovascular tissue that provides a more stable support/matrix for the further development of blood vessels and bone tissue [16,78,81]. Through reciprocal signalling, vasculature and bone mature side by side. Hypertrophic chondrocytes and cells of the osteoblastic lineage contribute to the secretion of vascular endothelial growth factor (VEGF) [84], a pro-angiogenic factor that, in synergy with several bone morphogenic proteins (BMPs), increases the recruitment of MSCs and encourages their

differentiation towards osteoblasts [16]. Stimulated ECs proliferate, migrate, and develop into structures to form new vessels and restore the blood flow in the callus. The vasculature surrounding and growing into the provisional fibrous tissue is vital for its replacement by the hard callus, as it enables sufficient delivery of oxygen and nutrients required for this endochondral ossification and helps to convey osterix-positive osteoprogenitor cells from the perichondrium into the metaphysis, contributing to osteoblastogenesis inside the bone [14,16,19,78,79,84–86]. Finally, the provisional woven bone is remodelled through repetitive tissue resorption and deposition cycles and replaced by a functional lamellar bone [14,78,79].

The vascular network can be formed via two processes, angiogenesis and vasculogenesis, which are often incorrectly interchanged despite their substantial differences. Vasculogenesis employs the endothelial progenitor cells (EPCs), which are obtained from different sources. The recruitment of EPCs is governed by molecular (cytokines) and environmental (hypoxic) factors. These cells then further differentiate into mature endothelial cells and develop *de novo* (new) blood vessels [15–17,82]. The importance of vasculogenesis in the onset of vascularization during embryonic development has been known for decades, but recent studies confirmed its role also postnatally [15]. Angiogenesis, on the other hand, utilizes the existing vasculature and is the dominant vessel formation process in tissue repair and tumour growth. It differentiates between two mechanisms of network growth: sprouting and splitting of the blood vessels [15–17,82]. The latter process, also called intussusceptive angiogenesis, is usually observed in well-perfused regions undergoing morphological changes, such as remodelling or growth. In contrast, areas with no or very little blood supply, such as wounds, are characterised by proliferative branching (sprouts) from the remaining vasculature, thus forming a new capillary network [15,87,88]. Sprouting angiogenesis, the prevailing revascularization mechanism for fracture healing, is defined by the following stages which are also illustrated in Figure 15.

1) Firstly, the basement membrane of the blood vessels, which together with mural cells (vascular smooth muscle cells and pericytes) prevents ECs from leaving their designated location in the vascular wall, must be degraded to liberate the ECs. Major biomolecular factors of this phase include matrix metalloproteinases, which define the extent of the membrane degradation and at the same time are responsible for the secretion of angiogenic factors, such as vascular endothelial growth factor (VEGF), fibroblast growth factor (FGF), and transforming growth factor beta (TGF-β), as well as activation of relevant angiogenic chemokines [15,20,89].
2) The sprouting angiogenesis is characterized by endothelial cells of distinct (but reversible) function and morphology. The new branches comprise of tip and stalk cells. The establishing capillaries are guided by mildly proliferative tip cells, contain many filopodia and navigate the new vessels toward a relevant (angiogenic) stimulus (hypoxia, biochemical gradient) [15,20].
3) The new endothelial branch is initially formed as a solid cord without a lumen. The growth and branching of the new vessel are mainly determined by the proliferation of stalk cells, which, in contrast to tip cells, are characterized by fewer filopodia [15]. Moreover, they are responsible for the production of the basement membrane and the establishment of junctions with neighbouring cells [15,89].
4) Stalk cells are responsible not only for the elongation of the branches but also for lumen formation, which is achieved by the tubular arrangement of these cells. Past studies introduced two mechanisms, in which the lumen is formed either by “cell hollowing” or “cord hollowing”.

The “cell hollowing” theory works on the assumption that the intracellular vacuoles of adjacent endothelial cells connect, thus creating inner space. The more recent “cord hollowing” theory, on the other hand, explains the lumen formation with cells acquiring a distinct phenotype, subsequent rearrangement of neighbouring cells, and lumen opening as a result of repulsive forces on the established inner membrane [15,89,90].

5) Once the lumen is established, the blood flow initiates. The contiguous tubular branches are then coalesced, forming an interconnected network. The new vasculature is then corrected through remodelling and pruning; the nutritional demands give rise to small and large vessels, whereas local levels of oxygen and VEGF determine apoptosis of some ECs to accomplish the optimal vascular density [15,89].

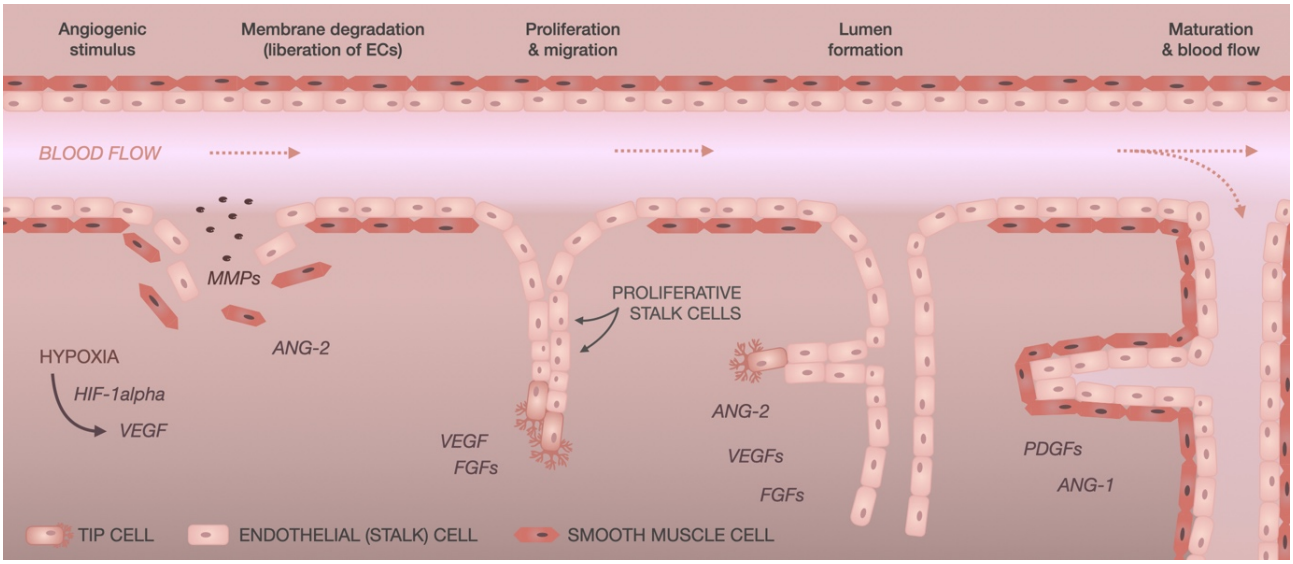

Figure 15. An illustration of sprouting angiogenesis. The presence of different factors (hypoxia, HIF1- alpha, VEGF) can initiate angiogenesis, which is divided into 4 stages: 1) In the first stage, the membrane degrades resulting in the liberation of ECs; 2) The cells proliferate and migrate, thereby establishing new branches of the vascular network; 3) The new branches are initially formed without a lumen and are hollowed in a subsequent stage; 4) The new endothelium matures, and blood flow is established through the new vessels.

The blood vessel formation process is governed by several biomolecular factors. The hypoxic conditions and increased lactate levels, characteristic for the hematoma and callus at the site of an injury, stabilize expression of hypoxia-inducible factor 1 alpha (HIF1-α) [14,17,18,83]. According to some studies conducted in mice, the increased expression of HIF1-α was associated with hyper-vascularisation, while its depletion resulted in delayed callus formation [17]. HIF1-α drives expression of VEGF, which promotes both the angiogenic and vasculogenic processes [17,18], and more than 60 factors related to adaptation in hypoxic conditions [90]. VEGF is secreted by many cells, including MSCs, osteoblasts, hypertrophic chondrocytes, but also inflammatory cells [16]. It stimulates proliferation and sprouting of endothelial cells and its expression attracts EPCs towards the site of injury. Studies have shown that inhibition or deficiency of VEGF is reflected in the reduced angiogenic potential, healing ability, and quality of the newly formed tissue [14,17,18,78,83]. Platelet endothelial cell adhesion molecule (PECAM1), also known as cluster of differentiation 31 (CD31), is an adhesion and signalling molecule expressed by vascular cells. In coordination with other molecules, it has been

demonstrated to promote the migration of endothelial cells while also ensuring maintenance of cellular integrity in terms of proper barrier function (permeability) and cell-cell junctions [91].

8.3.2 Voltage transients during PEO and SEM-EDS surface analyses

The curves of voltage-time (V-t) response recorded during the PEO surface treatments are portrayed in Figure 16 and the curve characteristics are summarized in Table 1.

The chemical composition of the surfaces was analysed by EDS and the results are summarized in Table 2. The analysis confirmed presence of Ti, Al, V, O, Ca and P on both PT and PT-Sr samples. The high content of detected Ti and O implied that TiO_2, resulting from oxidation of the titanium substrate, is a major constituent of the growing oxide layer. The presence of phosphor and calcium was more profound on PT samples, with the latter due to its possible substitution by strontium atoms on PT-Sr samples.

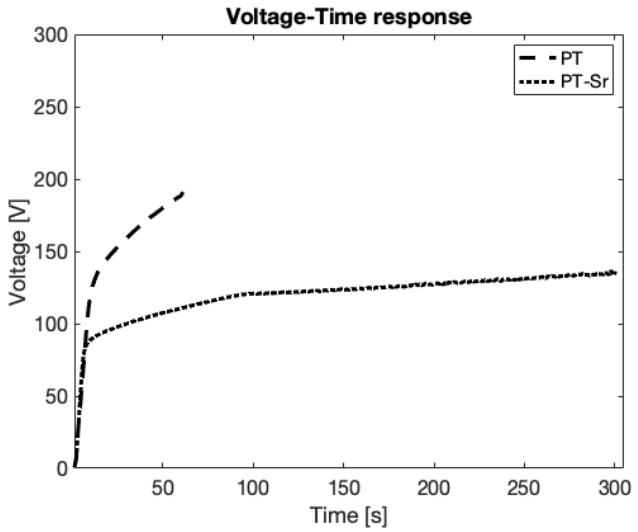

Figure 16. The evolution of the voltage during the PEO process in electrolytes without (PT) and with (PT-Sr) strontium.

Table 1. Summary of V-t curves characteristics PT and PT-Sr samples and values of electrolytes' conductivities.

	Average initial voltage increase rate [V/s]	Breakdown voltage [V]	Time to breakdown voltage [s]	Final voltage [V]	Electrolyte's conductivity [mS/cm]
PT	10 ± 0.5	139 ± 4.5	14 ± 1.5	192 ± 6.5	10.43 ± 0.1
PT-Sr	8 ± 1.0	90 ± 1.0	11 ± 1.5	138 ± 3.5	34.10 ± 0.1

Table 2. Chemical composition of the PT and PT-Sr surfaces generated through PEO treatment [wt.%] obtained from EDS analysis.

	C	O	Al	P	Ca	Ti	V	Sr
PT	18.0 ± 0.90	41.0 ± 2.50	2.0 ± 0.15	4.5 ± 0.50	7.0 ± 1.20	26.5 ± 2.50	1.0 ± 0.45	-
PT-Sr	16.5 ± 0.65	35.0 ± 1.90	2.0 ± 0.50	0.22	1.5 ± 0.20	34.5 ± 4.50	2.2	13.0 ± 1.50

8.4 Additional assays with HUVECs seeded on strontium releasing implants

8.4.1 Visualization of the implant coverage by HUVECs using DAPI staining

Implants with/without strontium seeded with 300 000 cells were cultured for 1, 4 and 7 days. After each timepoint, the cells were washed with PBS, fixed with 4 % PFA + 1 % GA in PBS (PBS; pH 7.4) for 15 minutes and washed twice with demi-water. Aliquot DAPI staining solution was added to each well, followed by 5 minutes of incubation in the dark. The stained cells were then imaged on a fluorescent microscope (Carl Zeiss, Axiovert 200M).

Before establishing an optimized seeding protocol with fibronectin, DAPI staining was used to visualize the occupation of PT and PT-Sr implants by HUVECs. The samples were incubated for 1, 4 and 7 days and the number of cells found on the surfaces was compared. The results summarized in Figure 17 show a decreasing trend of cellular coverage occupation throughout the period. On day 1, both PT and PT-Sr implants were fully covered and only few detached cells were seen on the bottom of wells. After 4 days, the surfaces clearly contained fewer cells, while the number of cells found in the wells increased. On day 7, only few cells were still attached on the implants, while many seemed to have left the implant's surface and prefer proliferating on the bottoms of the wells in the proximity of PT and PT-Sr implants. There was no observed difference in the effects of PT and PT-Sr surfaces on the cellular coverage.

8.4.2 Gene expression

Implants with/without strontium seeded with HUVECs were cultured for 1, 4 and 7 days. As control, HUVECs at the density of 10 000 cells/well were seeded in a 48-well plate. For RNA isolation, RNeasy Micro Kit (Qiagen, Cat No. 74004) was used. At each timepoint, cells were washed with PBS before proceeding with RNA isolation protocol.

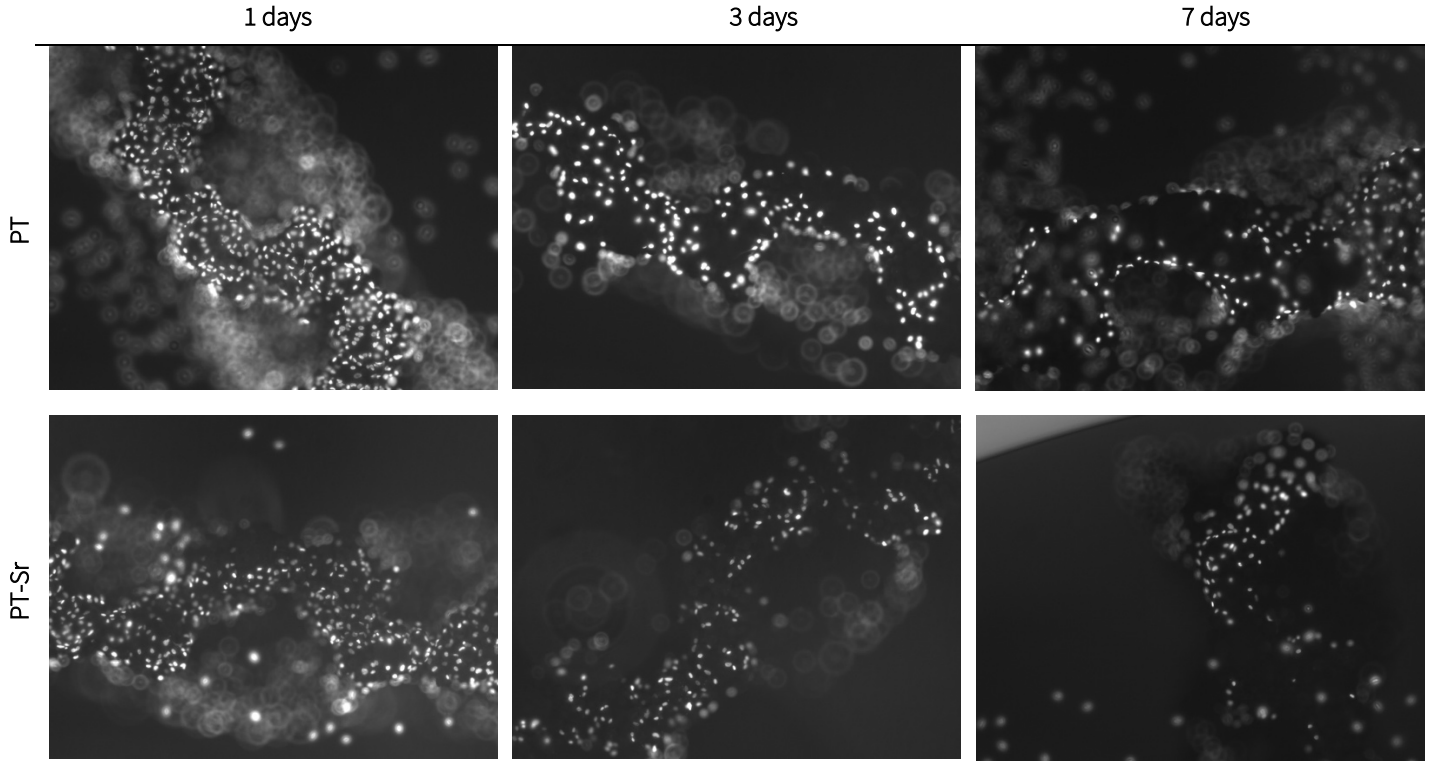

Figure 17. DAPI staining of HUVECs on PT and PT-Sr implants 1, 4 and 7 days.

RNA isolation

The implants with cells were transferred to 0.2 ml PCR Eppendorf tubes, 150 µl of RLT buffer was added and the tubes were vortexed to homogenize the suspension. Cells grown in a monolayer in a 48-well plate were added 75 µl of RLT buffer and scraped with a pipet tip. The cell lysates were pipetted to mix, transferred to 1.5 ml tubes and homogenized by vortex. One volume of 70 % ethanol was added to the lysate and mixed by pipetting. The samples were then transferred to a RNeasy MinElute spin columns placed in 2 ml collection tubes and centrifuged for 15 seconds at 10 000 rpm (8000 g). The flow through was discarded, 350 µl of RW1 buffer was added to each RNeasy MinElute spin column, and the samples were centrifuged for 15 seconds at 10 000 rpm. After that, 10 µl DNase I stock solution and 70µl RDD buffer was added to each sample, followed by an incubation at room temperature (20 – 30°C) for 15 minutes. An aliquot of 350µl RW1 buffer was added to each column and they were centrifuged for 15 seconds at 10 000 rpm. In the next step, 500µl RPE was pipetted in the spin columns, they were centrifuged for 15 seconds at 10 000 rpm and the flow through was discarded. Subsequently, 500µl of 80% ethanol was added to the column and centrifuged for 2min at 10 000 rpm. The columns were placed in new 2 ml collection tubes and centrifuged at full speed for 5 minutes. The columns were placed in new 1.5 ml tubes, 10 µl RNase-free water was added directly to the centre of
the spin column membrane and samples were centrifuged for 1 min at full speed (this step was repeated).

Nanodrop

In order to determine the amount of obtained RNA, nanodrop test was performed (QIAxpert and QIAxpert Software v 2.4, Qiagen). From each sample, 2 µl of resuspended RNA was pipetted on the slide and inserted into the QIAxpert. The amount of RNA in the sample was automatically measured. Based on the results, concentrations of all samples were corrected to 500 ng/10 µl for further use.

cDNA synthesis

In the first step, 2 µl of gDNA removal mix, template RNA and RNase-free water were mixed in total volume of 15 µl containing 500 ng of RNA. The mix was then incubated at 45°C for 2 minutes. Reverse transcription enzyme and reverse transcription mix, 1 and 4 µl respectively, were then added to each sample. In a -RT sample deprived of reverse transcriptase, 1 µl of reverse transcription enzyme was substituted with 1 µl of RNase free water. The samples were then incubated at 25°C for 3 minutes, at 45°C for 10 minutes and finally at 85°C for 5 minutes to inactivate the enzyme. The tubes were then stored on ice before proceeding with qRT-PCR.

qPCR

Primers crossing an exon-exon boundary for specificity were generated and ordered from Sigma Aldrich and Integrated DNA Technologies (Table 3). Primer working stocks (10 µM) were created with RNAse free water. Total reaction volume of 20 µl per sample was obtained by combining 10 µl of 2x QuantiNova SYBR green PCR master mix, 1.4 µl of forward primer, 1.4 µl of reverse primer, 2.2 µl of RNase-free water and 5 µl of cDNA. The Samples were then thoroughly mixed and pipetted in 50 µl Rotor X gene PCR Tubes. A protocol with a 2-minute incubation at 95°C followed by 35 incubation cycles of 95°C for 5 seconds and 60°C for 10 seconds was selected.

Table 3. Forward and reverse primer sequences of the 3 tested angiogenic genes and a housekeeping gene.

Primer	Primer sequence forward	Primer sequence reverse
RPL30	ACAGCATGCGGAAAATACTAC	AAAGGAAAATTTTGCAGGTTT
VEGFA	ACAACAAATGTGAATGCAGACCA	TACCGGGATTTCTTGCGCTT
HIF1A	GAGGGAGCCAGCGCTTAG	ACTTATCTTTTTCTTGTCGTTCGC
PECAM1	ATACTCTAGAACGGAAGGCTCC	ATGTCCTTCCAGGGATGTGC

RNAse-free water and a -RT sample were used as controls. RPL30 was used as a housekeeping gene and used for correction of the tested genes. The forward and reverse primer sequences of the 3 angiogenesis related genes (VEGFA, HIF1A, PECAM1) and a housekeeping gene (RPL30) are summarized in Table 3.

The results of the performed qPCR are depicted in Figure 18. Unfortunately, the low amount of extracted RNA yielded insufficient number of replicates per condition. Moreover, the possible variability of cells per implant resulted in relatively large errors. Those challenges were discussed in section 6.

8.4.3 Gene selection for ELISA

The cells were also tested on secretion of angiogenesis-related signalling molecules VEGF and FGF-21. VEGF is an essential promotor of angiogenesis, guiding/driving expression of more than 60 factors related to adaptation in hypoxic conditions [90]. It stimulates proliferation and sprouting of endothelial cells and studies have shown that inhibition or deficiency of VEGF is reflected in the reduced angiogenic potential, healing ability, and quality of the newly formed tissue [14,17,18,78,83]. FGF-21 has been inherently associated with cellular survival. A link between its inhibition and compromised growth and proliferative and migration capacity of endothelial cells has been identified, indicating its vital role in angiogenesis [92–94].

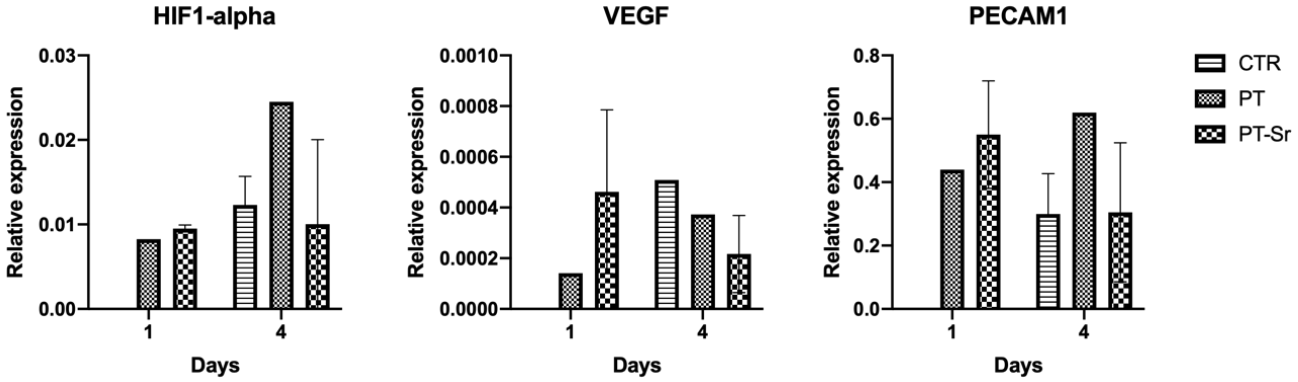

Figure 18. Expression of angiogenesis-related genes HIF1-alpha, PECAM1 and VEGF by HUVECs on day 1 and 4 after seeding. The analysis revealed relatively large standard deviation for the samples, resulting most likely from differences in cell number between replicates. Moreover, insufficient amount of cellular materials led to low number of replicates per condition, questioning reliability of those results.